HYPERSONIC RESEARCH ENGINE PROJECT - PHASE II
AEROTHERMODYNAMIC INTEGRATION
MODEL DEVELOPMENT
ELEVENTH INTERIM TECHNICAL DATA REPORT
DATA ITEM NO. 55-4.11
10 SEPTEMBER THROUGH 9 DECEMBER 1970
NASA CONTRACT NO. NAS1-6666

Document No. AP-70-7035

GARRETT

AIRESEARCH MANUFACTURING COMPANY
A DIVISION OF THE GARRETT CORPORATION
9851-9951 SEPULVEDA BLVD. • LOS ANGELES, CALIFORNIA 90009
TELEPHONE: SPRING 6-1010, ORCHARD 0-0131 • CABLE: GARRETTAIR LOS ANGELES

AIRESEARCH MANUFACTURING COMPANY
Los Angeles, California

HYPERSONIC RESEARCH ENGINE PROJECT - PHASE II
AEROTHERMODYNAMIC INTEGRATION
MODEL DEVELOPMENT
ELEVENTH INTERIM TECHNICAL DATA REPORT
DATA ITEM NO. 55-4.11
10 SEPTEMBER THROUGH 9 DECEMBER 1970
NASA CONTRACT NO. NAS1-6666

Document No. AP-70-7035

Number of pages 74

Original date 6 January 1971

Prepared by Engineering Staff

Edited by L. F. Jilly

Approved by E N Harris
Edward N. Harris
HRE Program Manager

Revision	Date	Pages Affected (Revised, Added, Eliminated)

FOREWORD

This interim technical data report is submitted to the NASA Langley Research Center by the AiResearch Manufacturing Company, Los Angeles, California. The document was prepared in accordance with the guidelines established in paragraph 5.7.3.2.2 of NASA Statement of Work L-4947-B (Revised).

Interim technical data reports are generated on a quarterly basis for major program tasks under the Hypersonic Research Engine (HRE) Project. Upon completion of a given task effort, a final technical data report will be submitted.

This document presents a detailed technical discussion of the development of the Aerothermodynamic Integration Model (AIM) engine for the period 10 September through 9 December 1970.

ACKNOWLEDGEMENTS

Acknowledgements for contributions to this document are hereby extended to the following persons:

L. Kado K. Mastin	Technical Coordination
L. Pearson	Aerodynamics
A. Vuigner C. Young	Heat Transfer Analysis
W. Flieder	Stress Analysis
A. Heller	Design
W. Latto	Development

CONTENTS

ILLUSTRATIONS

ILLUSTRATIONS (Continued)

ILLUSTRATIONS (Continued)

TABLES

1. SUMMARY OF STATUS

1.1 OVERALL ENGINE DESIGN

The analytical effort expended during this reporting period was directed toward (1) analyzing the latest inputs of possible test conditions and their impact on hardware; (2) a review of structural capabilities of the AIM unit; (3) analyzing coolant flow paths, heat transfer, and associated problems relative to the cowl leading edge tip section; and (4) redefining requirements of flow-calibrating the air-metering duct.

1.2 HARDWARE STATUS

Fabrication of the various components of the AIM unit has progressed satisfactorily with the exception of the cowl leading edge assembly. Six components were completed and assembly of the centerbody was initiated. Completion of the remaining components is scheduled for early part of the next reporting period.

The estimated percentages of completion of the various components of the AIM unit are as follows.

Component	Percent Complete	
	Details	Subassembly
Spike assembly	100	100
Inner shell	100	100
Nozzle plug	100	100
Cowl leading edge	100	90
Outer shell	100	100
Nozzle shroud	100	100
Outer cowl body	100	100
Air metering duct	100	99
Combustor exit instrumentation support assembly	90	75
Temperature probe		100
Pressure probe		100

1.3 TESTS

1.3.1 Cowl Leading Edge Flow Test

Additional flow tests were performed on the cowl leading edge tip section incorporating a redesigned flow-divider section.

Desired coolant flow distribution and pressure-drop profile was achieved.

1.3.2 Seal Tests

Various gasket materials and sealants were evaluated to achieve the sealing desired at the interface of the strut/inner shell and outer cowl body/crossover manifold.

2. PROBLEM STATEMENT

The objective of the Aerothermodynamic Integration Model (AIM) is to verify the feasibility of integrating various analytical and experimental data obtained for the design of the Hypersonic Ramjet Engine, and to evaluate the overall engine performance of this design. The design of this model will be directed to evaluating aerodynamic characteristics without major concern for the structural life of the model.

3. TOPICAL BACKGROUND

The Aerothermodynamic Integration Model (AIM) will be a water-cooled, ground-test model of the Hypersonic Research Engine.

The nomenclature used to describe the various aerodynamic surfaces of this engine is shown in Figure 3-1.

General design guides to be followed in the design of the AIM will be (1) the aerodynamic contours of the AIM will be those obtained from component testing wherever possible, (2) the surface temperature of the engine will be dictated by the maximum metal temperature allowable for structural integrity and by requirements of preventing boiling of the water used as the coolant, and (3) in order that the engine may be tested over the range from Mach 3 to 8, the inlet spike will be mechanized to permit translation.

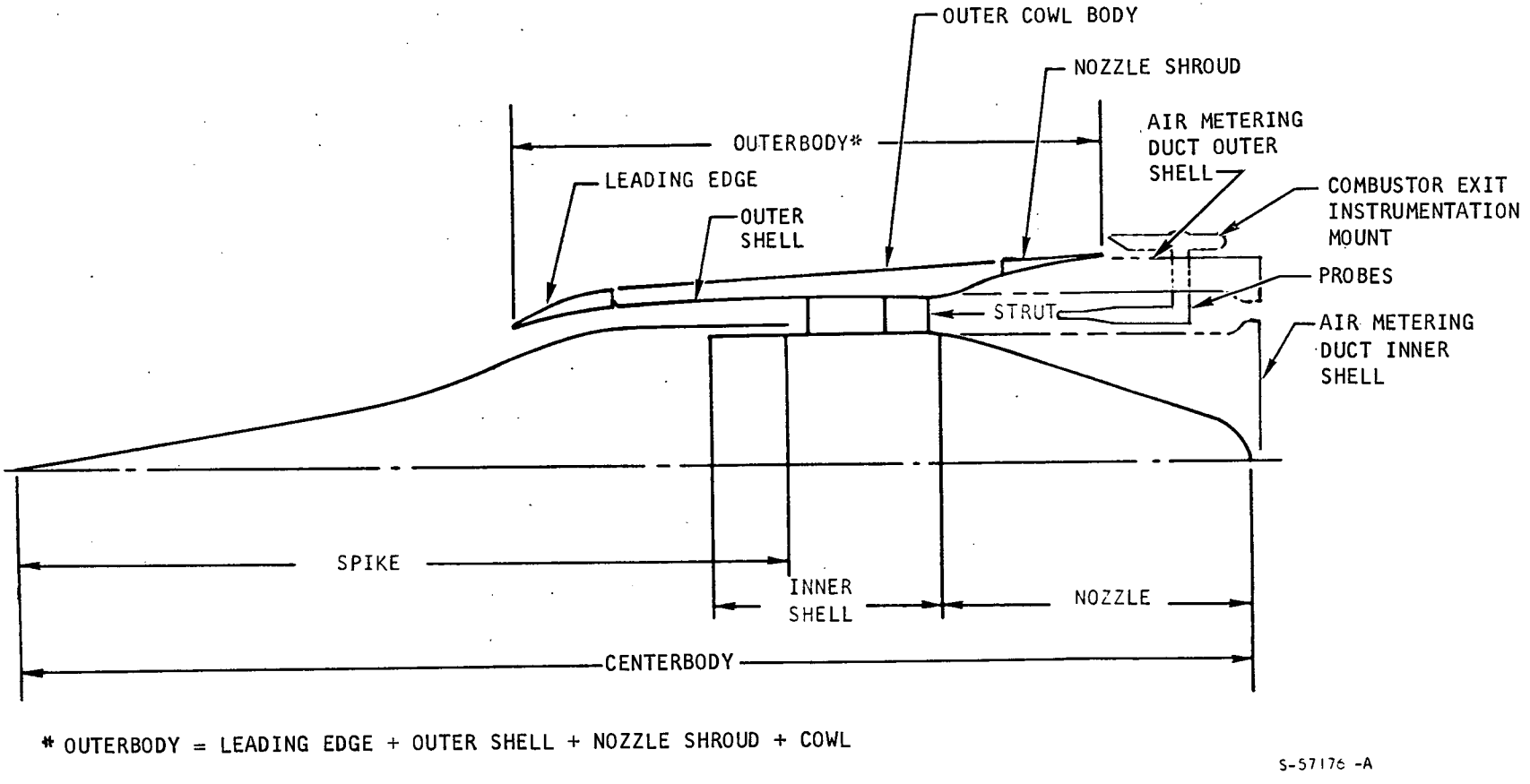

Figure 3-1. Aerothermodynamic Integration Model Nomenclature

4. OVERALL APPROACH

The basic design concepts previously submitted were used in the component layout drawing. However, due to the diverse requirements imposed upon the design to satisfy the considerations of thermal analysis, structural design, mechanical design and manufacturing techniques, tests will be conducted to determine the internal aerodynamic performance over Mach number range of 5.0 to 7.0. The effects of varying inlet air total pressure and temperature, fuel-air ratio, inlet spike position, and combustion mode will be investigated. All tests will be conducted with clean air. The measured performance will have to be corrected to account for heat removed by the water-cooling system.

Tests will be performed to

(a) evaluate the inlet-combustor interaction and stability

(b) evaluate the performance of the positive ignition system

(c) identify conditions when autoignition is feasible

(d) demonstrate combustion mode transition

(e) evaluate inlet and combustor performance

(f) determine overall engine performance

(g) determine engine operating characteristics with feasible variations in fuel equivalence ratio

(h) determine nozzle performance for the purpose of substantiating the predicted overall engine performance, including chemical kinetic effects

5. ANALYTICAL DESIGN

The analytical effort expended by the aerodynamic group was directed toward (1) defining the aerodynamic profiles within the air-metering duct, (2) re-evaluating the method of performing calibration tests on the air-metering duct, and (3) evaluating the effects of shock interaction at the trailing end of the AIM unit.

The analytical effort expended by the stress group was directed toward re-examining the structural capabilities of the AIM components based on the latest inputs of operational requirements.

5.1 AERODYNAMIC ANALYSIS

5.1.1 Air Metering Duct

Results of the analytical study will be compared with the test data obtained from the scaled model tests performed by NASA Langley, Hampton, Virginia.

Aerodynamic profiles within the air metering duct for test conditions are estimated as follows.

The variations in total pressure, total temperature, and velocity have been estimated for the AIM flowmeter duct. The calculation was made for Mach 7 conditions, assuming an exponential velocity profile of the form

$$\frac{u}{u_{\mathbb{C}}} = \left(\frac{r}{\delta}\right)^{1/N}$$, where u = local velocity, $u_{\mathbb{C}}$ = centerline velocity

r = distance out from the wall, δ = boundary layer thickness = one-half of the annulus height, and N = 7. A Crocco temperature distribution was further assumed with a ratio of wall-to-centerline temperature of 0.3. Resulting profiles are presented in Figure 5-1.

5.1.2 Air Metering Duct Calibration

A line drawing, approximately to scale, of a recommended flowmeter calibration rig is given in Figure 5-2. This is similar in concept to a flow-entrance section which was used in 1/3-scale nozzle testing earlier in this program.* The configuration includes a supersonic nozzle detailed in Figure 5-3. This nozzle simulates Mach 6-7 flow in terms of shock strength. The nozzle coordinates given in Figure 5-3 are from WADC TR 54-279, 1954, and may

*Reference FluiDyne Engineering Corporation Project 0585, March 1968, AiResearch Manufacturing Company P.O. 418-86801-7.

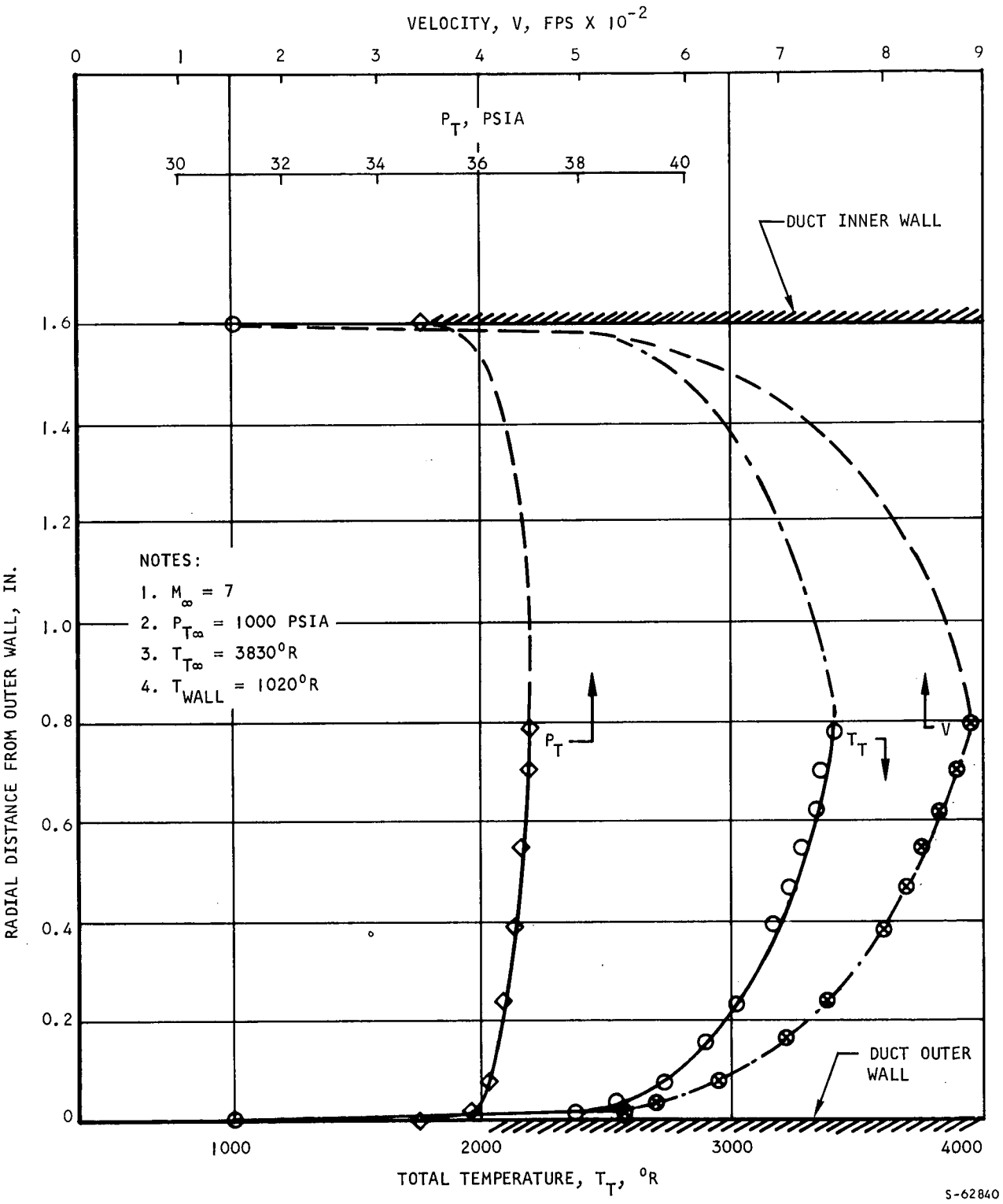

Figure 5-1. AIM Flowmeter Duct - Estimated Flow Profile

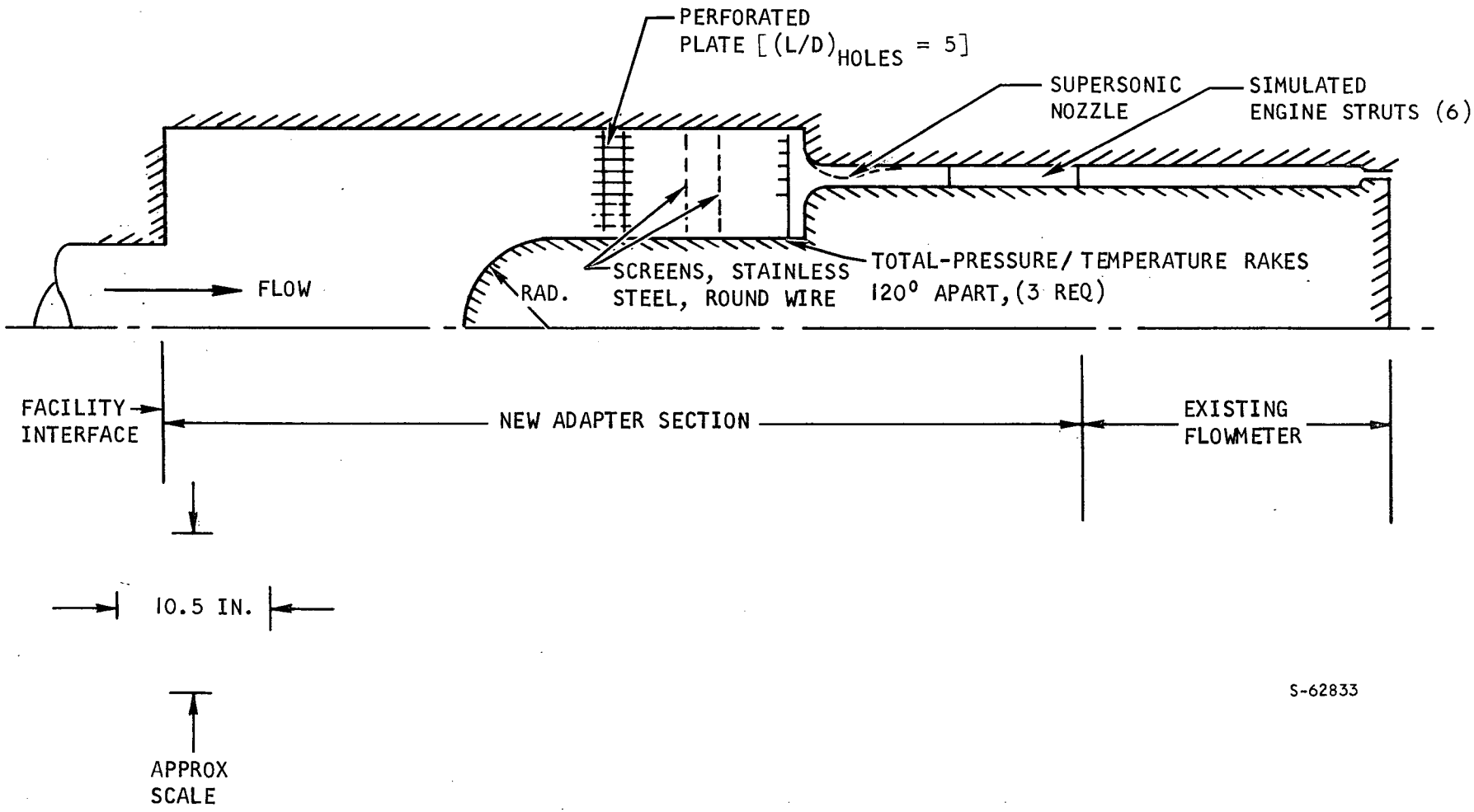

Figure 5-2. AIM Flowmeter Calibration Installation Schematic

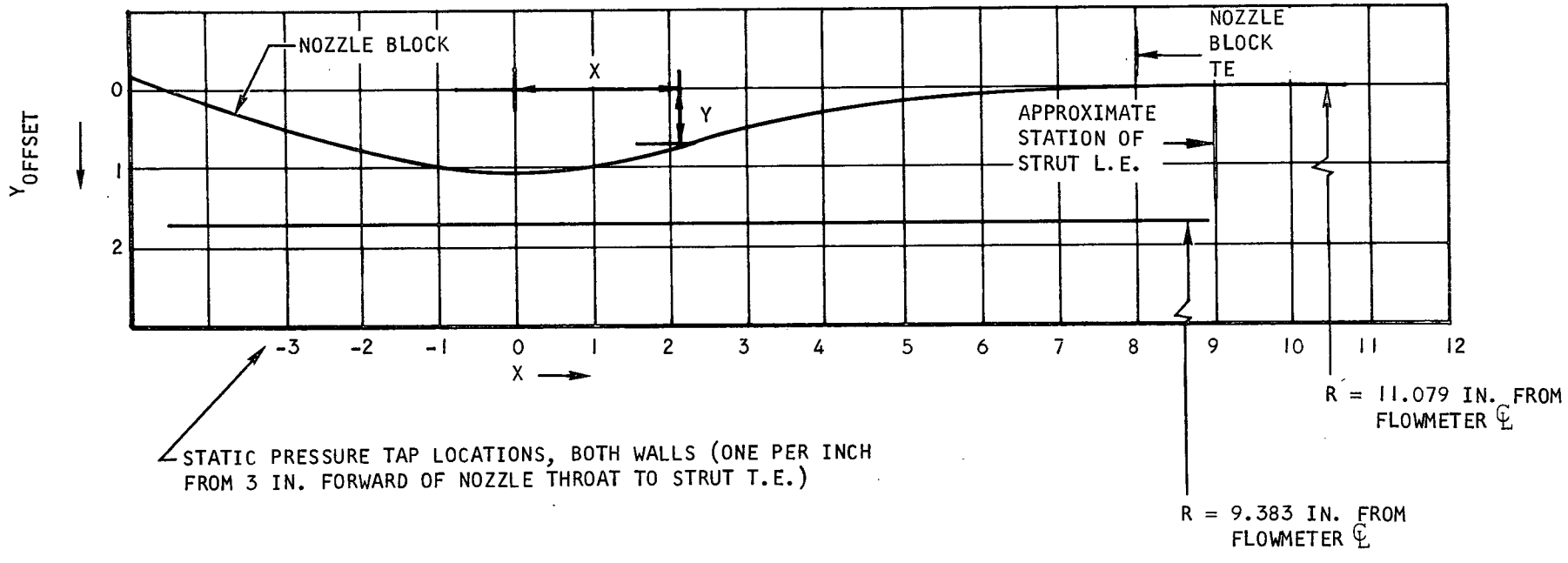

NOZZLE BLOCK COORDINATES, INCHES (THROAT LOCATED AT X = 0)

X	-2.900	-2.420	-1.710	-1.110	-0.620	-0.310	-0.125	-0.480	-0.001		
Y	0.520	0.680	0.872	0.981	1.034	1.053	1.056	1.056	1.056		
X	(+)0.046	0.122	0.277	0.462	0.707	1.131	1.400	2.710	4.770	6.810	8.010
Y	1.056	1.055	1.048	1.038	1.015	0.958	0.905	0.577	0.199	0.025	0.0

S-62838

Figure 5-3. AIM Flowmeter Calibration Rig Supersonic Nozzle

be inverted to the opposite wall of the annulus for better simulation by maintaining the implied relation of area vs distance.

The choke-plate and screens are designed to give total pressure losses of 67 percent and 10 percent, respectively. Parametric design data for these components are given in Figures 5-4, 5-5, and 5-6.

Reynolds number variations calculated for the Plumbrook test conditions are presented in Figure 5-7. The required flow conditions to simulate these Reynolds numbers with unheated air are tabulated in Table 5-I.

TABLE 5-I

FLOW CONDITIONS REQUIRED TO DUPLICATE PLUMBROOK REYNOLDS NUMBER USING COLD AIR SUPPLY

AIM Flowmeter Calibration	Maximum Re	Minimum Re
Re/X, per ft	1.8×10^6	0.13×10^6
$P_{T_{supply}}$, psia	56	4.0
$P_{discharge}$, psia	4.7	0.33
$T_{T_{supply}}$, (assumed), ^0F	100	100
Airflow, lb/sec	15.6	1.1
Volume flow, $ft^3/min.$	41,000	41,000

5.1.3 Facility Shock-Nozzle Interference

The effect of wind tunnel flow in terms of the shroud trailing shock structure has been evaluated. The shock structure is presented in Figure 5-8. Conclusions are as follows:

(a) Local pressure is the dominant index of whether shroud trailing shock will impinge on plug; local Mach No. has only secondary influence.

(b) Local pressure on rear face of shroud (15 deg) surface must exceed 10 tunnel atmospheres before shock impingement will occur.

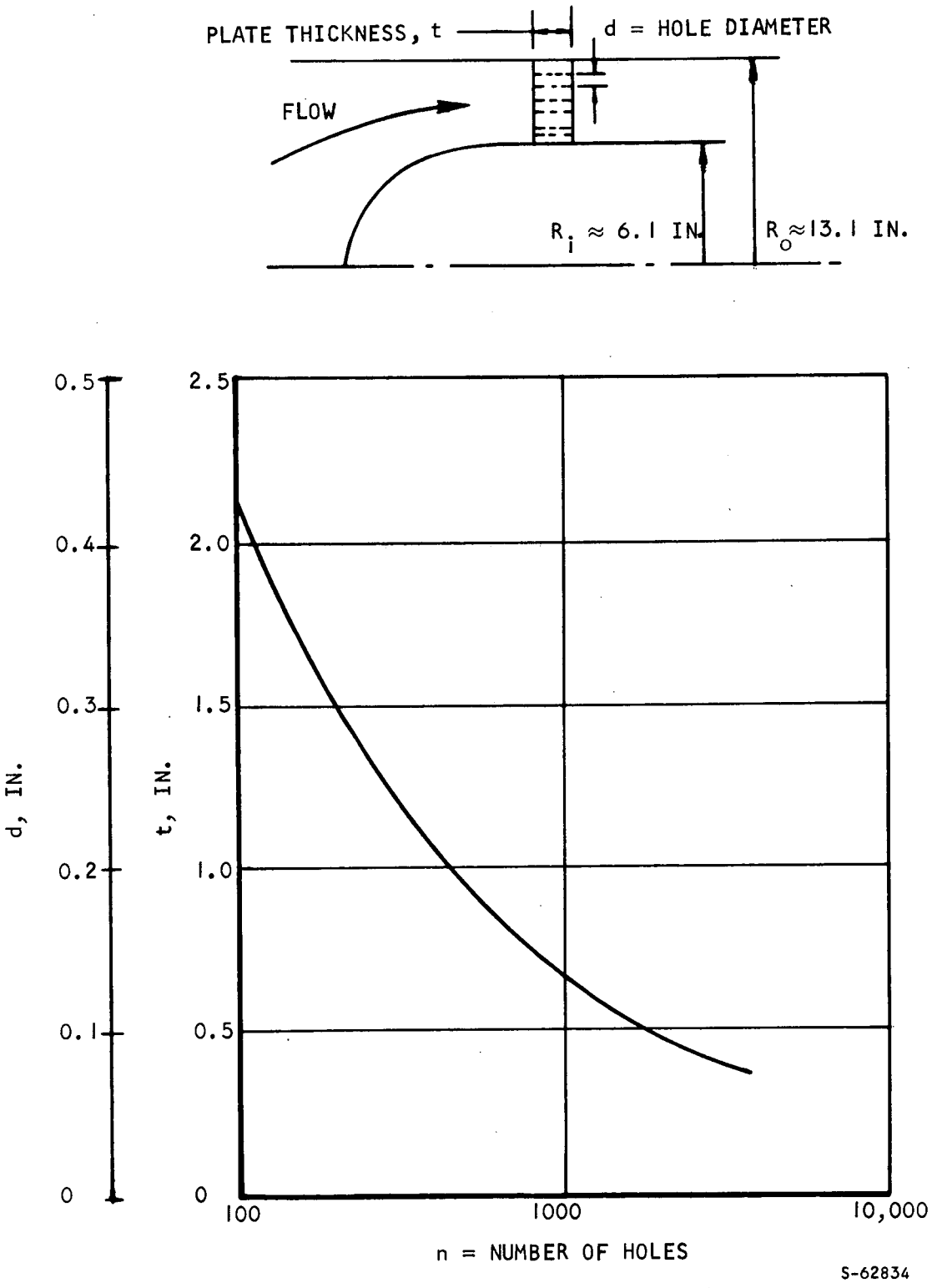

Figure 5-4. AIM Flowmeter Calibration Choke Plate

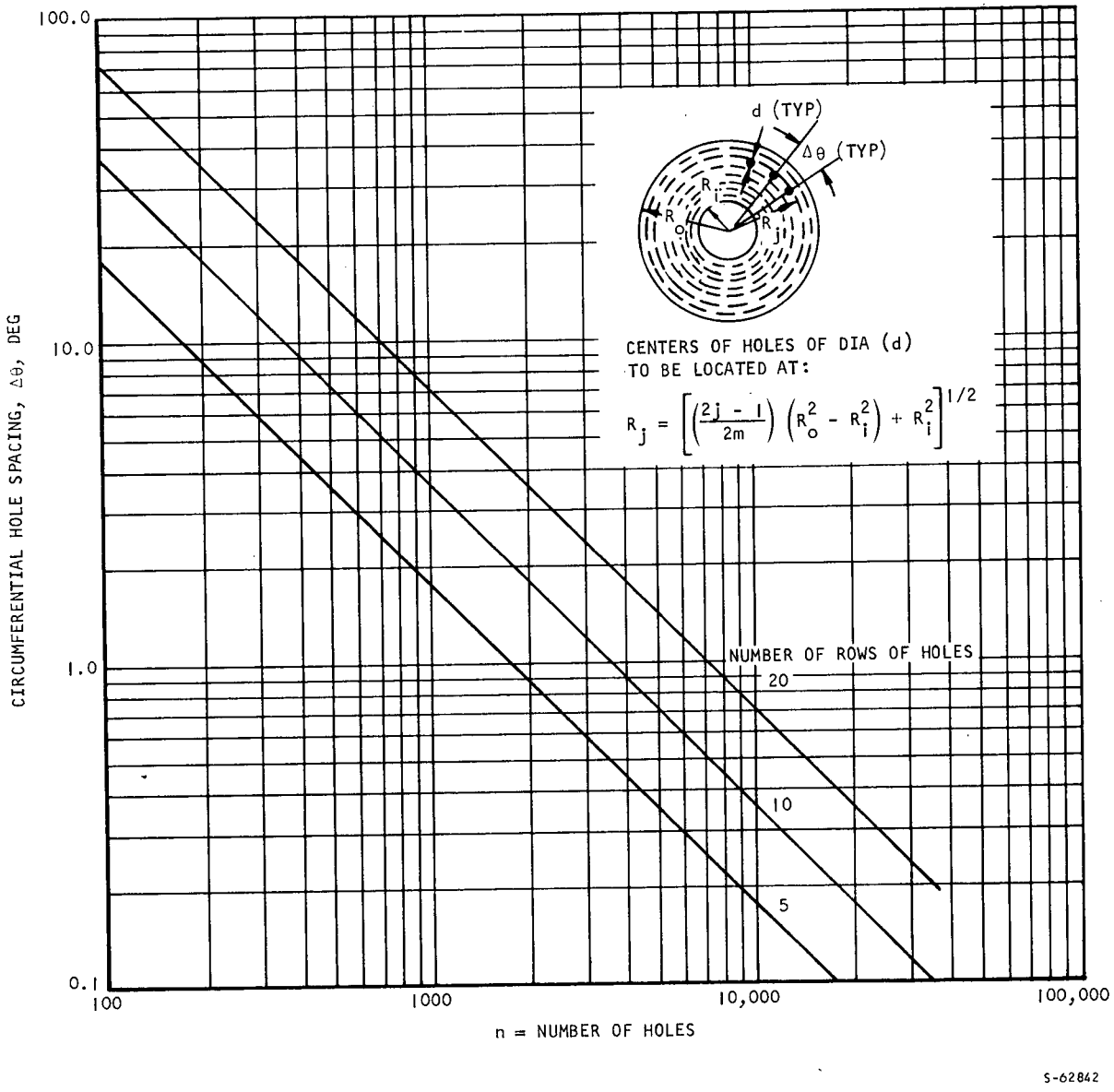

Figure 5-5. AIM Flowmeter Calibration Choke Plate

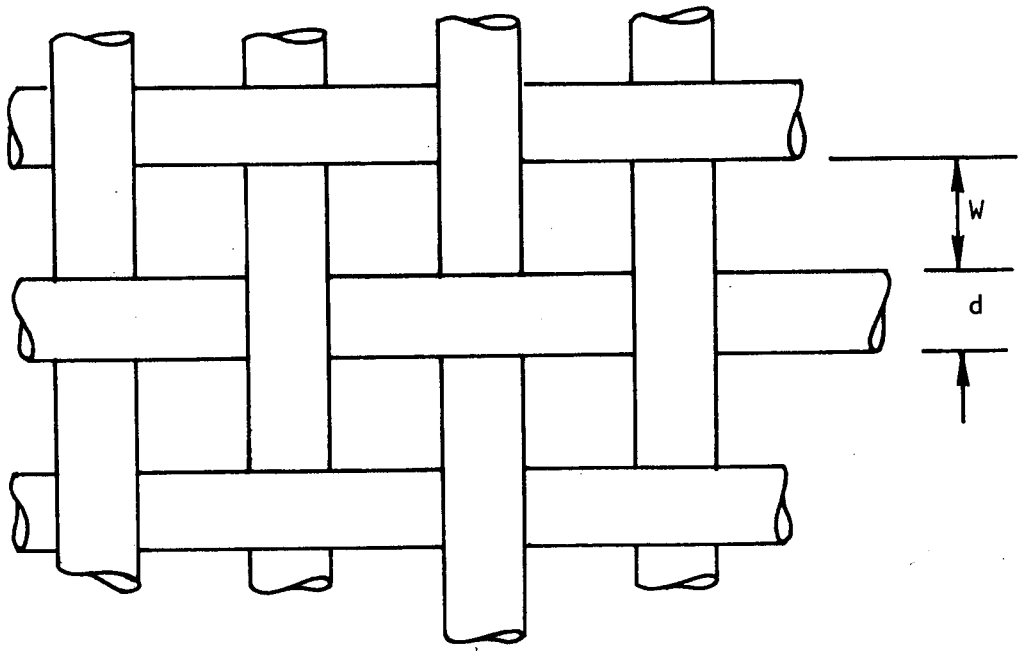

$\frac{d}{W} \approx 0.7$

MATERIAL: STAINLESS STEEL
ROUND WIRE

S-62835

Figure 5-6. Screen Mesh Requirements

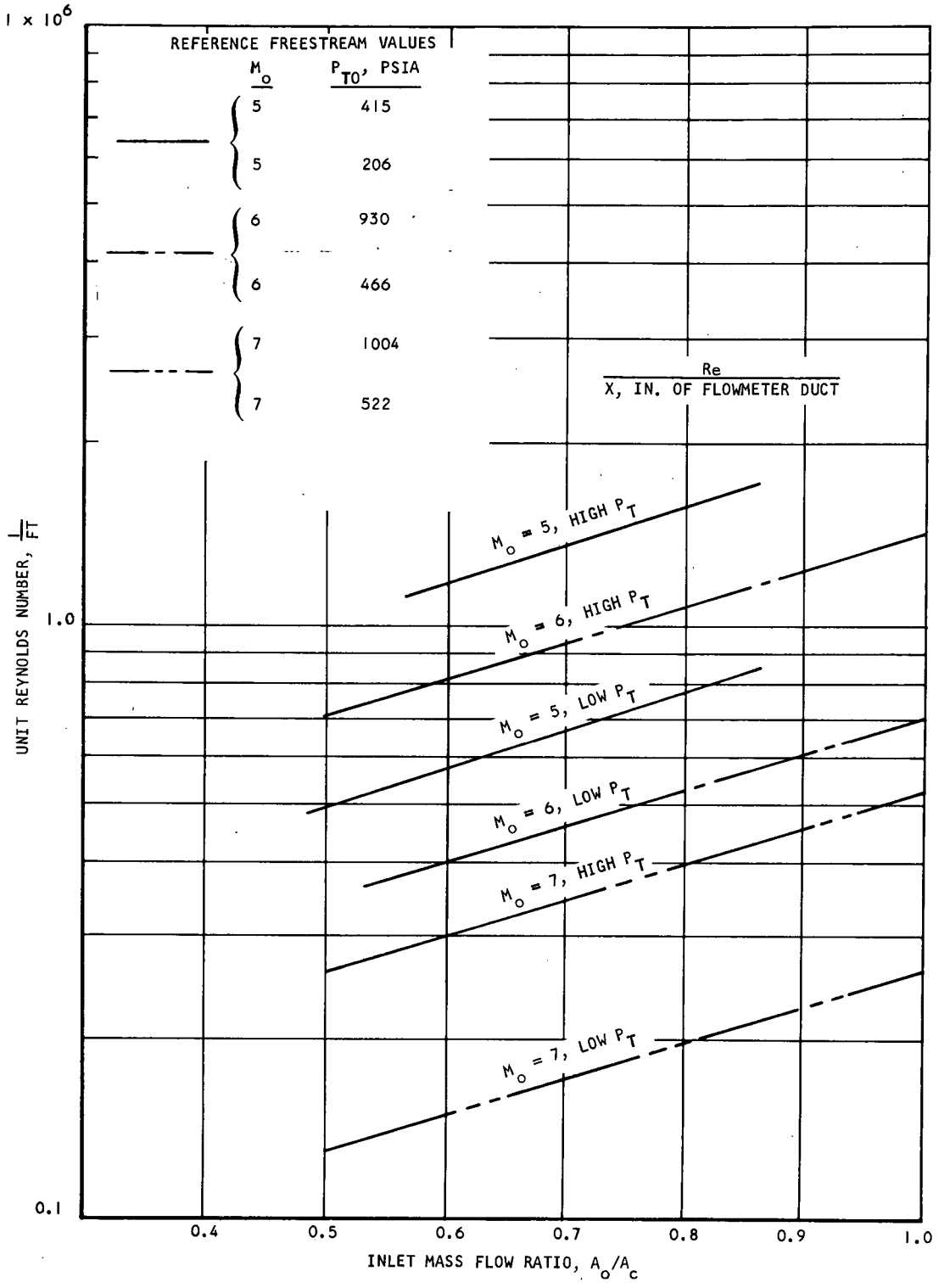

Figure 5-7. AIM/Plumbrook Test Unit Reynolds Number Variation

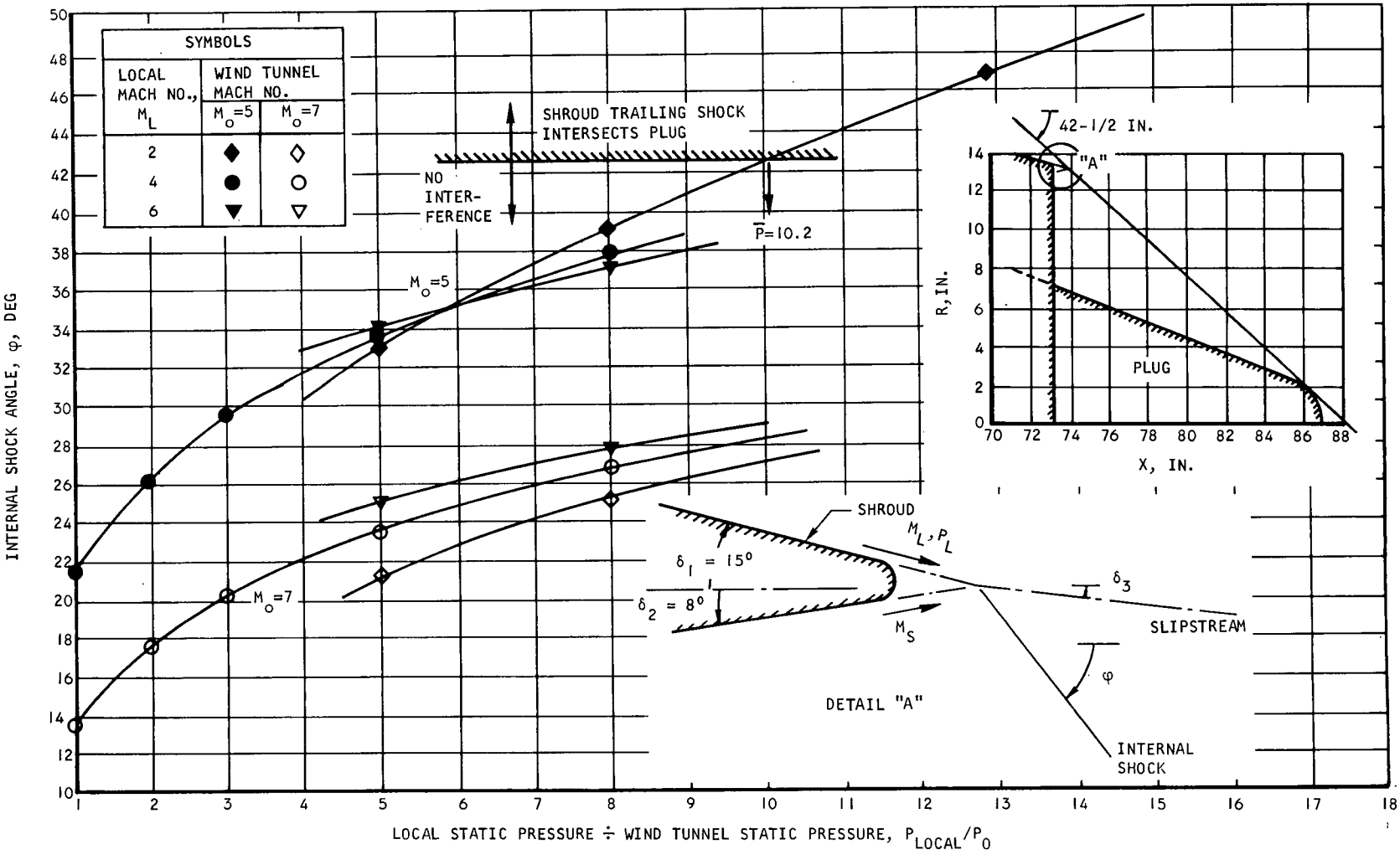

Figure 5-8. HRE/AIM Envelope of Shroud Trailing Shock Angles

(c) Tunnel Mach No. = 5 is design condition; M + 7 is much less likely to cause impingement.

(d) Shroud separation, rather than shock impingement on the plug, may be a problem at M = 5; probably not at M = 7 due to fixed-nozzle area ratio.

5.2 STRESS ANALYSIS

5.2.1 Engine Pressure-Containment Capability

A complete review was made of the entire AIM engine structure to assess the pressure-containment capability of the engine. For this analysis, the most current information was used regarding details of the fabricated hardware. The various parts of the engine and the related flow routes have been sketched and broken down into numerous discrete zones.

5.2.1.1 Outerbody Pressure Capability

The total flow routing for the outerbody is shown in Figure 5-9. The outerbody includes the cowl, the outer shell and the nozzle shroud. Flow enters the water inlet manifold at the aft end of the cowl outer surface, proceeds towards and around the leading edge, along the entire inner surface, around the nozzle shroud trailing edge, and finally to the outerbody exhaust water manifold. The flow route has been subdivided into 16 zones that are described and precisely located in Table 5-2. The pressure capabilities at the most severe operating condition are listed for each zone. As noted in Table 5-2, the outerbody has been designed for an operating pressure of 220 psi. The most critical areas are zones 8 and 14, with pressure capabilities of 240 and 250 psi, respectively.

5.2.1.2 Spike Pressure Capability

The spike cooling water flow route is depicted in Figure 5-10. The spike has been subdivided into eight structural zones. The flow enters through the struts and is carried to the spike inlet manifold. The water flows aft to the spike end and then flows forward to the tip. The flow rate exits to the innerbody.

The eight spike zones are described and located on Table 5-3. The spike has been designed for a maximum operating pressure of 200 psi at operating temperatures. The most critical areas are zones 4, 5, and 6 with pressure capabilities of 225 psi.

5.2.1.3 Innerbody Pressure Capability

The innerbody flow routing consisting of the inner shell and the nozzle plug is shown on Figure 5-11. This structure has been broken down into six discrete structural zones that are described and located on Table 5-4. The water flow from the spike outlet enters the innerbody at the front end and

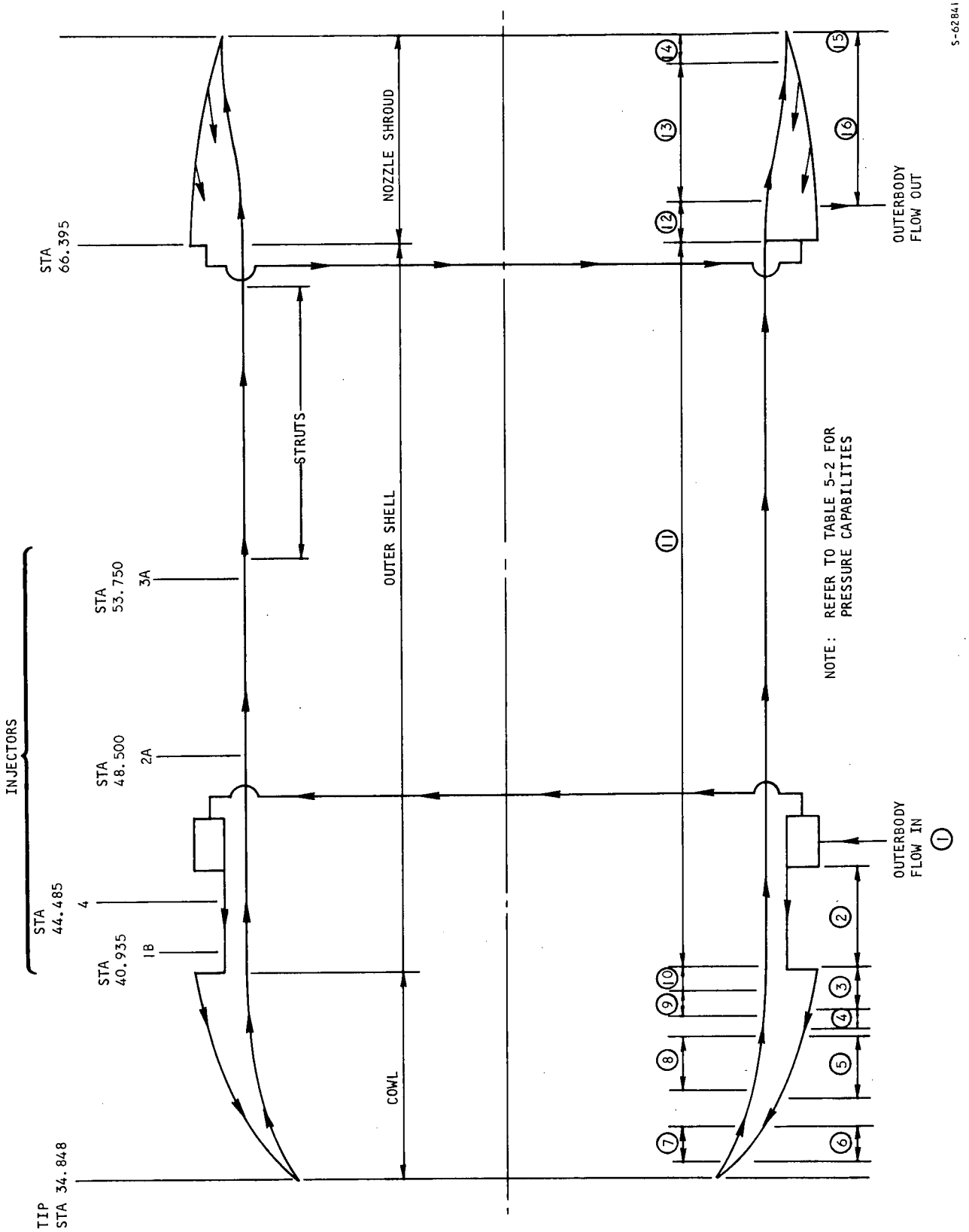

Figure 5-9. Outerbody Flow Route

TABLE 5-2

OUTERBODY PRESSURE-CONTAINMENT CAPABILITY

Zone (from Figure 5-9)	Zone Description	Station Location	Press. Capability at Operating Condition, psi
(1)	Inlet manifold	Sta. 51.0 to 46.0 (outside)	330
(2)	Sandwich-finned shell	Sta. 46.0 to 41.5 (outside)	>1000
(3)	Hastelloy ring water holes	Sta. 41.5 to 40.5 (outside)	>1000
(4)	Leading edge outer skin	Sta. 40.5 to 39.5 (outside)	> 500
(5)	Leading edge outer skin	Sta. 38.5 to 36.5 (outside)	300
(6)	Outer skin, leading edge	Sta. 35.7 to tip (outside)	300
(7)	Inner skin, leading edge	Tip to Sta. 35.7 (inside)	300
(8)	Leading edge inner skin	Sta. 36.5 to 38.5 (inside)	240
(9)	Leading edge inner flange	Sta. 39.6 to 40.5 (inside)	> 500
(10)	Outerbody hot skin	Sta. 40.5 to 41.3 (inside)	> 500
(11)	Outerbody hot skin finned shell	Sta. 41.3 to 66.4 (inside)	> 350
(12)	Nozzle shroud flange	Sta. 66.4 to 67.3 (inside)	500
(13)	Nozzle shroud inner skin	Sta. 68.2 to 71.4 (inside)	250
(14)	Inner skin, trailing edge	Sta. 71.4 to tip (inside)	250
(15)	Outer skin, trailing edge	Tip to Sta. 71.6 (outside)	350
(16)	Nozzle shroud, outer skin	Sta. 71.6 to 66.4 (outside)	350

P_{OPER} = 220 psi

P_{PROOF} = 330 psi

Minimum operating pressure capability = 240 psi

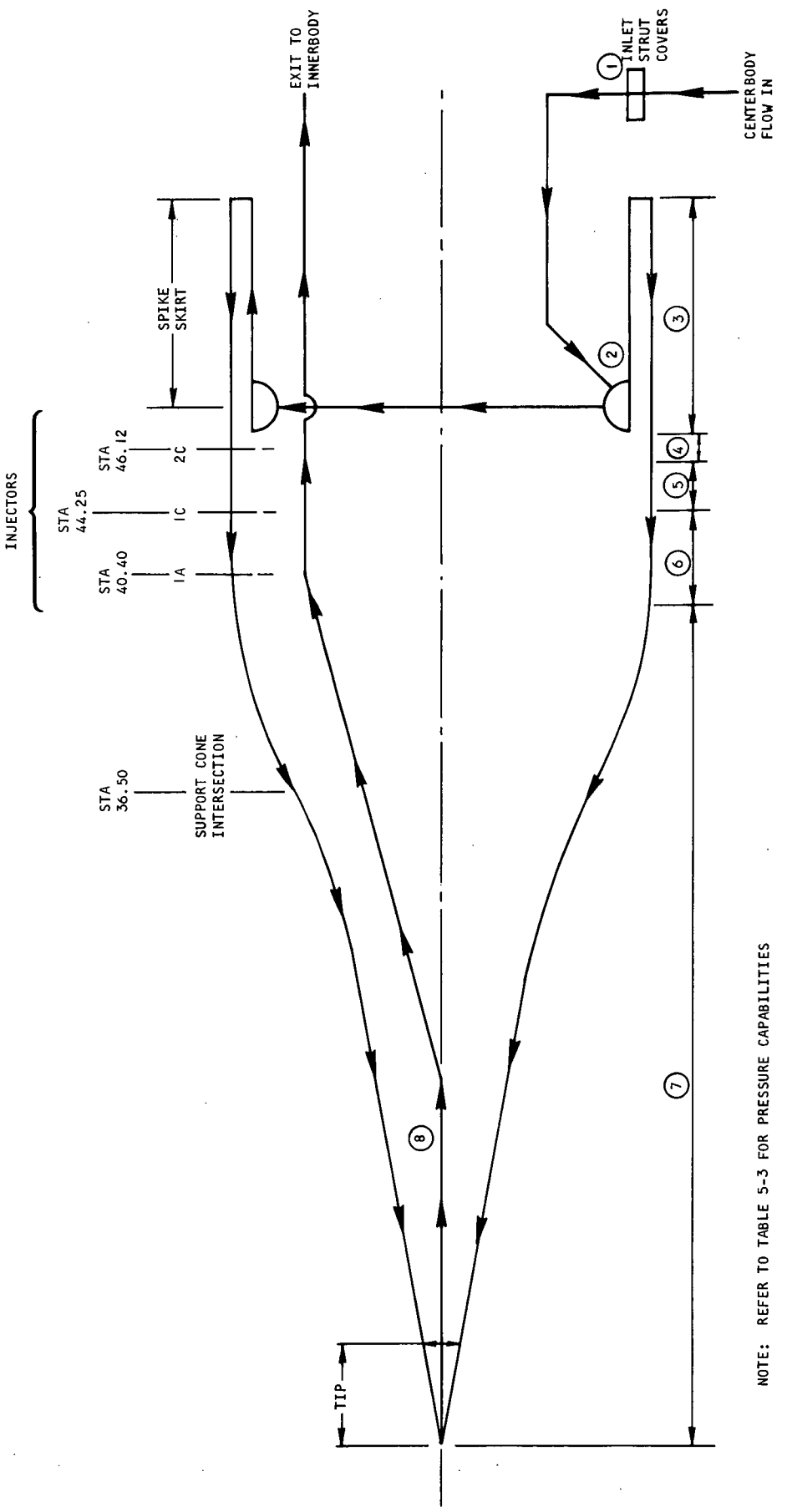

Figure 5-10. Innerbody Flow Route

TABLE 5-3

SPIKE PRESSURE-CONTAINMENT CAPABILITY

Zone (from Figure 5-10)	Zone Description	Location	Max. Operating Press. at Temp.
(1)	Inlet strut covers	Strut attachment area	>500
(2)	Spike inlet manifold	Sta. 48.25	>500
(3)	Spike skirt finned shell	Sta. 48.8 to 55.8	>425
(4)	Aft spike transition area	Sta. 48.8 to 47.85	225
(5)	Spike shell	Sta. 46.3 to 44.7	225
(6)	Spike shell	Sta. 44.7 to 40.6	225
(7)	Spike shell	Sta. 40.3 to tip	250
(8)	Spike plumbing to innerbody	Spike tip to innerbody	>300

P_{OPER} = 200 psi, P_{PROOF} = 300 psi

TABLE 5-4

INNERBODY/NOZZLE PLUG PRESSURE-CONTAINMENT CAPABILITY

Zone (from Figure 5-11)	Zone Description	Location	Press. Capability at Operating Temp., psi
(1)	Innerbody inlet header	Sta. 53.0	>500
(2)	Innerbody front cylinder	Sta. 49.9 to 55.8	225
(3)	Innerbody Strut and Panel Section	Sta. 55.8 to 65.0	225
(4)	Nozzle plug short cylinder	Sta. 66.0 to 67.1	>300
(5)	Nozzle plug cone	Sta. 68.0 to end	225
(6)	Nozzle plug exit plumbing	Sta. 85 to dump strut	>500

P_{OPER} = 200 psi, P_{PROOF} = 300 psi

Maximum pressure at capability operating temp. = 225 psi

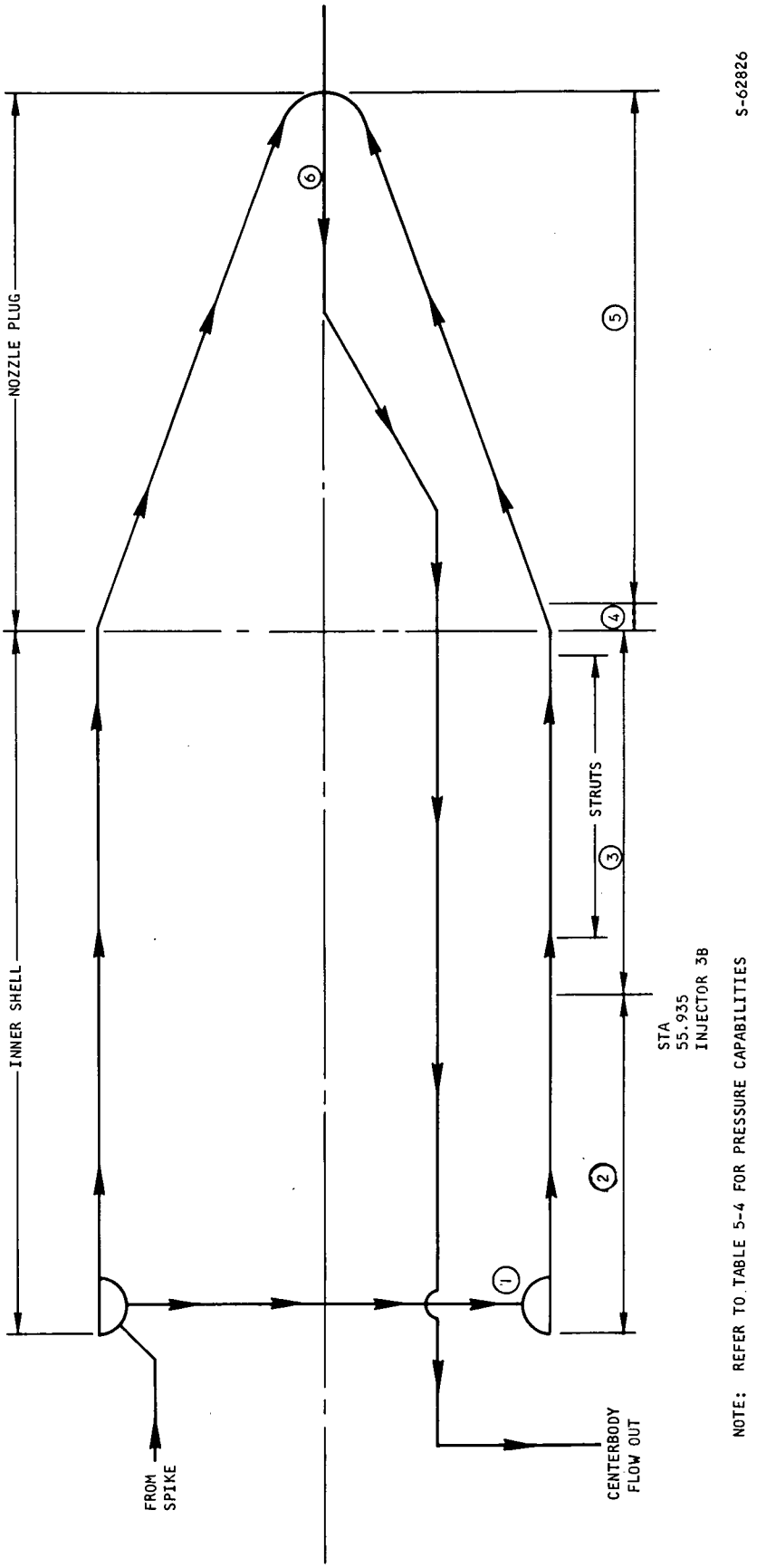

Figure 5-11. Innerbody Flow Route

then travels aft to the nozzle plug. This portion of the engine has been sized to contain a maximum operating pressure of 200 psi at operating temperatures. The most critical areas are the innerbody front cylinder and the innerbody curved panels between the strut sockets. The pressure-containment limitation for these regions is 225 psi.

5.2.1.4 Strut Pressure Capability

The strut cooling passages are shown on Figure 5-12. There are three distinct flow regions; the leading edge circuit, the strut body cooling holes, and the strut innerbody supply opening. The operating pressures for each of these zones and the containment capabilities are shown on the figure. In all three zones, the pressure capabilities are well in excess of the maximum operating pressures.

5.2.1.5 Outer Cowl Body

The outer cowl body is shown in Figure 5-13. There are four discrete flow circuits in this structure. The leading edge of the legs and the lower cowl has been denoted as zone 1. The maximum operating pressure at operating temperature is 245 psi, and the pressure-containment capability is in excess of 300 psi. The remaining three cooling circuits have containment capabilities of 200 psi compared to the rated operating pressures of 140 psi for each circuit.

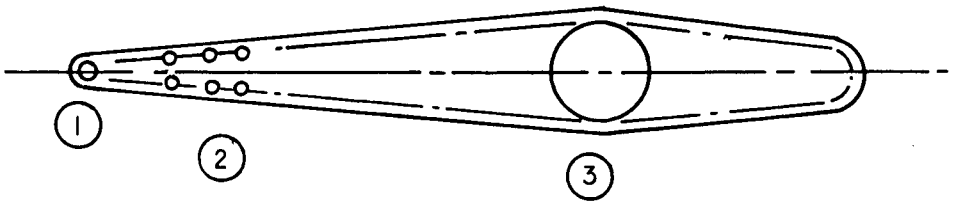

S-62802

(1) LEADING EDGE COOLING HOLE

P_{OPER} = 340 PSI

P_{PROOF} = 510 PSI

$P_{MAX.ALL.}$ ≥ 1000 PSI

(2) STRUT BODY COOLING HOLES

P_{OPER} = 350 PSI

P_{PROOF} = 525 PSI

$P_{MAX.ALL.}$ ≥ 1000 PSI

(3) INNERBODY SUPPLY HOLE

P_{OPER} = 200 PSI

P_{PROOF} = 300 PSI

$P_{MAX.ALL.}$ = 500 PSI

Figure 5-12. Strut Pressure-Containment Capability

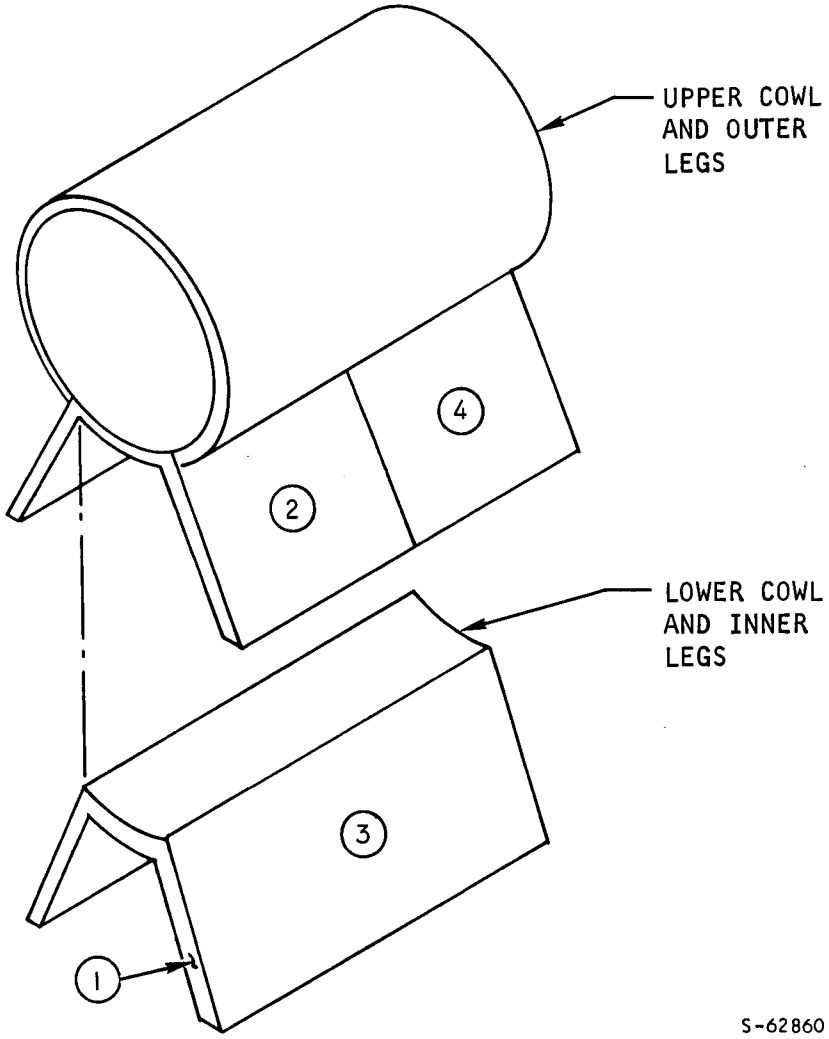

Zone	Description	Maximum Pressure Capability at Operating Temp	P_{OPER}	P_{PROOF}
(1)	Leg leading edge and front lower cowl	>300	245	370
(2)	Forward legs and upper cowl front	200	140	210
(3)	Legs and lower cowl rear	200	140	210
(4)	Legs and upper cowl rear	225	140	210

Figure 5-13. Outer Cowl Body Pressure Capability

6. DESIGN AND FABRICATION

6.1 DESIGN

Effort expended by the design group consisted of (1) completing the design and details of such items as brackets, supports for and routing of instrumentation lines, and layout of siphoning device for removing water from the AIM centerbody section; and (2) activities required to support manufacturing and assembly of the AIM components.

6.2 COMPONENT FABRICATION STATUS

6.2.1 Inlet Spike Assembly (Figure 6-1)

Fabrication phase of this component has been completed, including machining of the final contour. Brazing of the extension tubes of various hydrogen and coolant supply lines has been deferred to the assembly phase to facilitate assembly and improve schedules of subassembly and alignment-check. The spike assembly has been installed on the innerbody/actuator assembly and dimensional inspection has revealed that the alignments of these assemblies are well within required limits. The spike assembly has been removed from the actuator, and installation of the various manifolds, igniters, excitors, instrumentation leads, and associated components has been initiated.

6.2.2 Inner Shell Assembly

Fabrication of this component was completed during the last reporting period. The actuator assembly and its associated components were installed on this assembly; also the inner shell was aligned to the outer shell. Templates used to final contour-machine the struts, which support the inner shell to the outer shell, were obtained at this time. Subassembly phase of this component is progressing satisfactorily toward the targeted completion date.

6.2.3 Nozzle Plug Assembly

As reported in the previous AIM TDR, fabrication of this component has been completed.

6.2.4 Nozzle Shroud Assembly

Fabrication of this component is scheduled for early part of the next reporting period. Difficulties encountered in completing the component resulted from problems associated with welding Nickel-200 to itself as described in the previous AIM TDR.

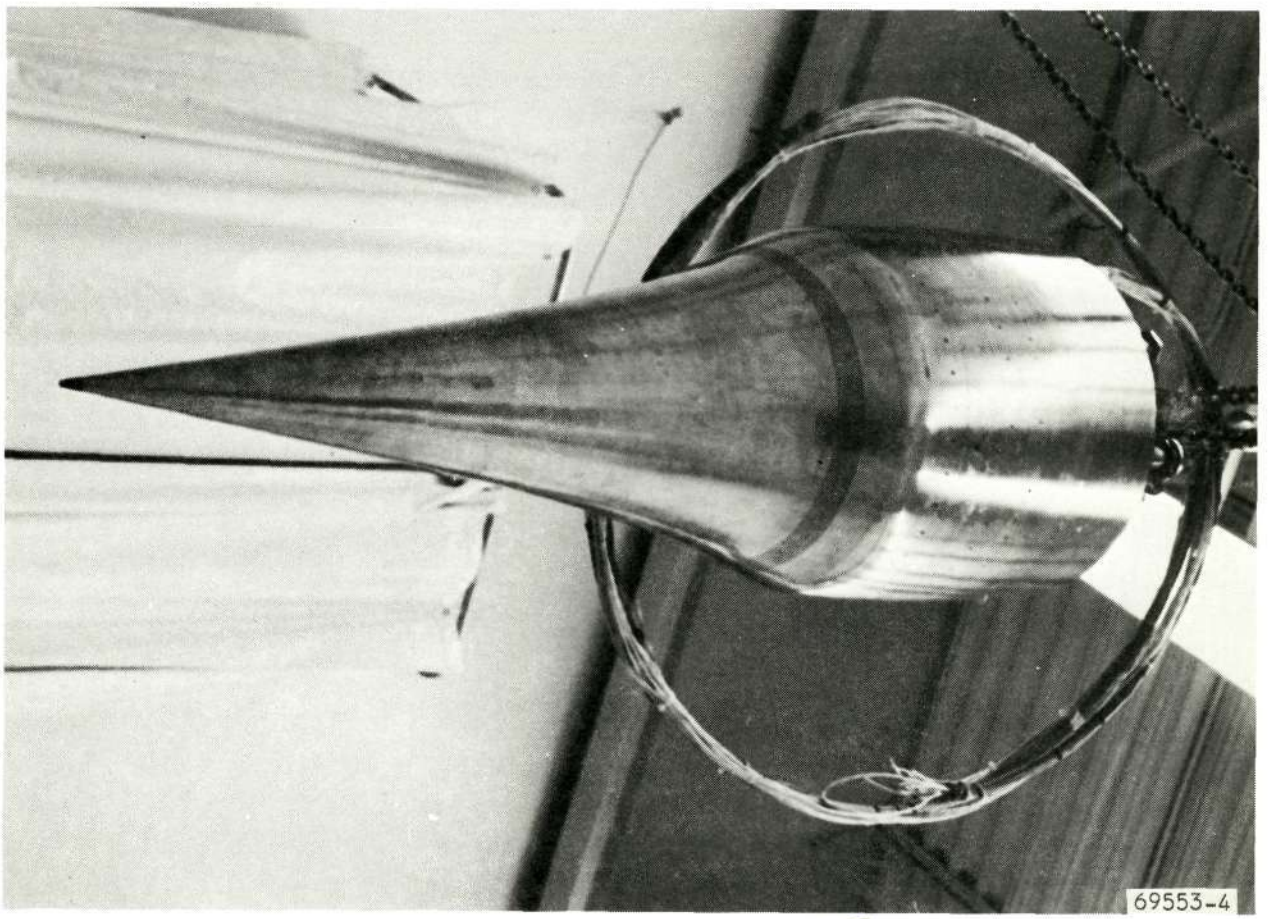

Figure 6-1. Inlet Spike Assembly

6.2.5 Outer Shell Assembly

Fabrication of this component was completed during this reporting period, including final contour-machining of the strut sockets and aerodynamic contour. Installation of manifolds used to supply fuel to the igniter assembly was deferred to improve schedules of fit/check and initiation of final contour-machining of the struts used to align the centerbody to the outerbody.

6.2.6 Cowl Leading Edge Assembly

Fabrication of this component has been delayed as a result of (1) metals joining problems described in the previous TDR, and (2) maldistribution of the coolant flow around the tip section, also described in the previous TDR.

Further testing was performed and configuration of the flow divider has been defined (see Section 7 of this report). A revised flow divider has been installed in the tip section and fabrication is proceeding satisfactorily.

6.2.7 Air Metering Duct

Fabrication of the air-metering duct plug assembly was completed during this reporting period. Fabrication of the air-metering-duct shroud assembly was delayed due to problems encountered during the brazing operation. Variance in the section thickness of the three concentric shells (see Figure 6-2), resulted in damage to the outer shell and instrumentation installed at this end. Thermocouples were installed in selected areas to control the rate of heating and cooling. It is believed that the heavy masses and extremely large diameter resulted in difficulties. Design changes were incorporated to remedy this condition.

6.2.8 Combustor Exit Instrumentation Mount Assembly

Fabrication of this assembly is progressing satisfactorily. Welding of the inner shell to the outer shell with all instrumentation leads installed within the ring was completed. Fabrication of the channeled-leg section is progressing satisfactorily, with completion of this assembly scheduled for the next reporting period.

6.2.9 Instrumentation Probes (Figure 6-3)

Fabrication of ten temperature-sensing probes, PN 950594, and six pressure-sensing probes, PN 950593, was completed during this reporting period.

6.2.10 Igniter Assembly (Figure 6-4)

Fabrication of the igniters and functional testing of these igniters was completed in this period.

Figure 6-2. Air-Metering Duct Plug

Figure 6-3. Air-Metering Duct Shroud

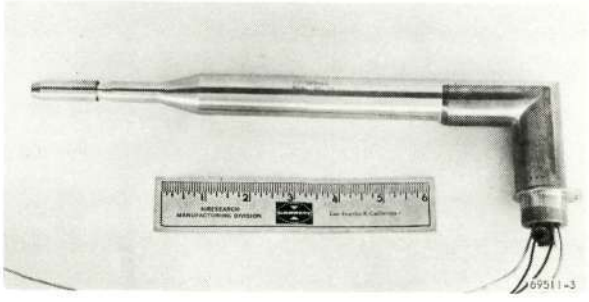

a. PN 950593 Temperature Probe

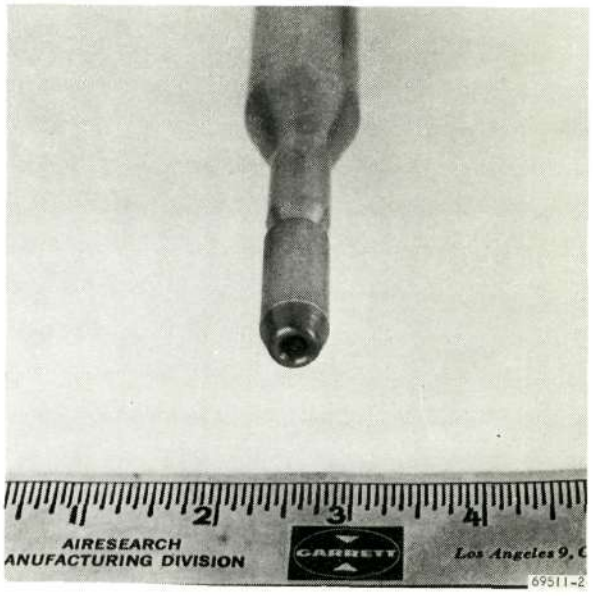

b. Tip Section of PN 950593 Temperature Probe

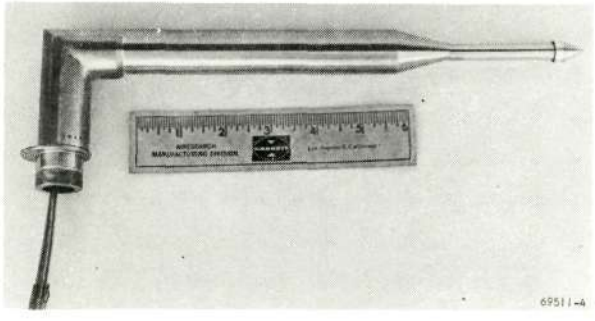

c. PN 950594 Pressure Probe

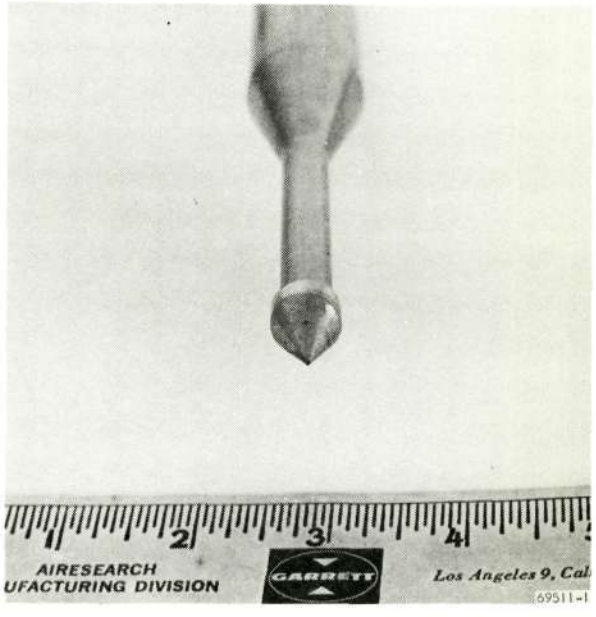

d. Tip Section of PN 950594 Pressure Probe

F-12849

Figure 6-4. Temperature and Pressure Probes

7. TESTS

7.1 COWL LEADING EDGE COOLANT FLOW TESTS

Tests of a full-scale cowl leading edge and seven ten-times-scale cowl leading edge models were described in the last report. A flow divider configuration was selected for additional testing based on these data. The results of this testing is described in this section.

7.1.1 Segmented Full-Scale Model Tests

A segment, 1.61 in. long, of the full-scale cowl leading edge was fitted with a flow-divider configuration derived from configuration 6 of the 10X-scale tests. This divider is shown in Figure 7-1. The design flow for this model is 18.3 gpm. A piece of 0.003-in.-thick foil was spot-tacked to the flow divider aft support in such a manner as to cover up the bypass holes in the divider. The purpose of the foil was to block off the bypass holes and thereby obtain a flow calibration of the 2-3 pressure drop for tip flow only. The test model was instrumented as before at three stations. A test fixture was fabricated from plastic so that visual observations could be made of the flow. During early testing with this fixture, cavitation was visible in the flow passage adjacent to the entrance and exit of the fins which support the forward end of the flow divider. Tests were conducted where the back pressure to the model was varied and the flow to the test fixture held constant. The overall model pressure drop and the 2-3 pressure drop decreased with increasing back pressure all the way to design operating pressure. Internal leakage of the test fixture was suspected; therefore, the clamping force supplied to the test fixture was increased and a shift in data was noted. It was found that when the fixture was disassembled, and reassembled, the data would not repeat; therefore, the plastic test fixture was abandoned. Although the metered flow was not equal to the model flow, due to internal test fixture leakage, qualitative data were obtained based on visual observations of cavitation. The results of these observations are shown in Figure 7-2. The model configuration of Figure 7-2 had the bypass holes covered. At the tip design flow (50 percent) the data indicated that visual cavitation is suppressed by an inlet pressure of approximately 40 psi.

A test fixture made of aluminum and steel was fabricated and developed to the point where the data did not indicate significant leakage. The fixture could be disassembled and reassembled without a significant change to the data. It was found that when data shifts were observed, a small amount of dirt had been trapped in the fins, and after disassembly and cleaning, the data repeated. Figures 7-3, 7-4, and 7-5 show the measured model pressure drops as a function of back pressure at constant flow with the bypass holes covered by the 0.003-in.-thick foil. The 2-3 pressure drop appears to be a reliable

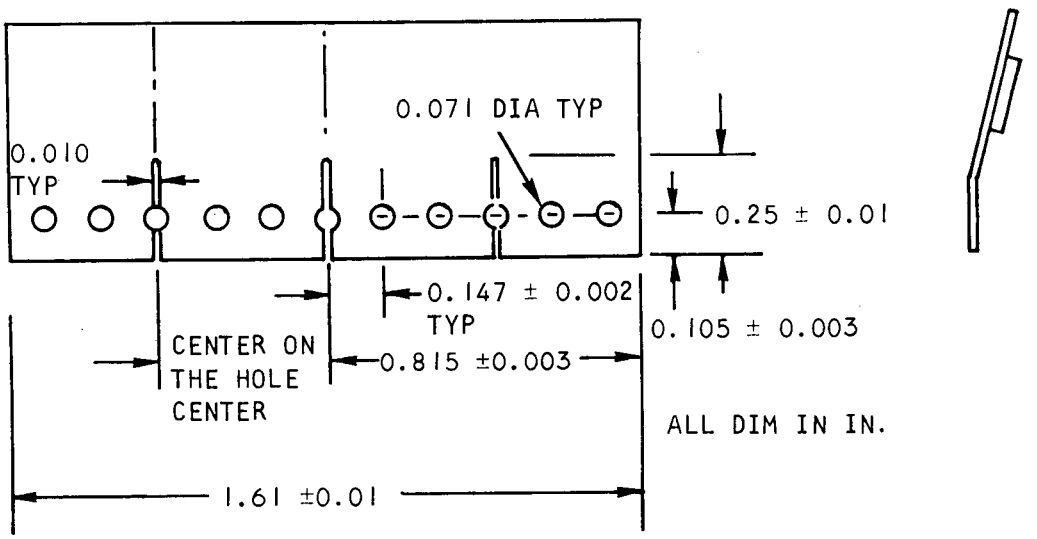

Figure 7-1. Flow Divider for Segment of Full-Scale Cowl Leading Edge Test Model

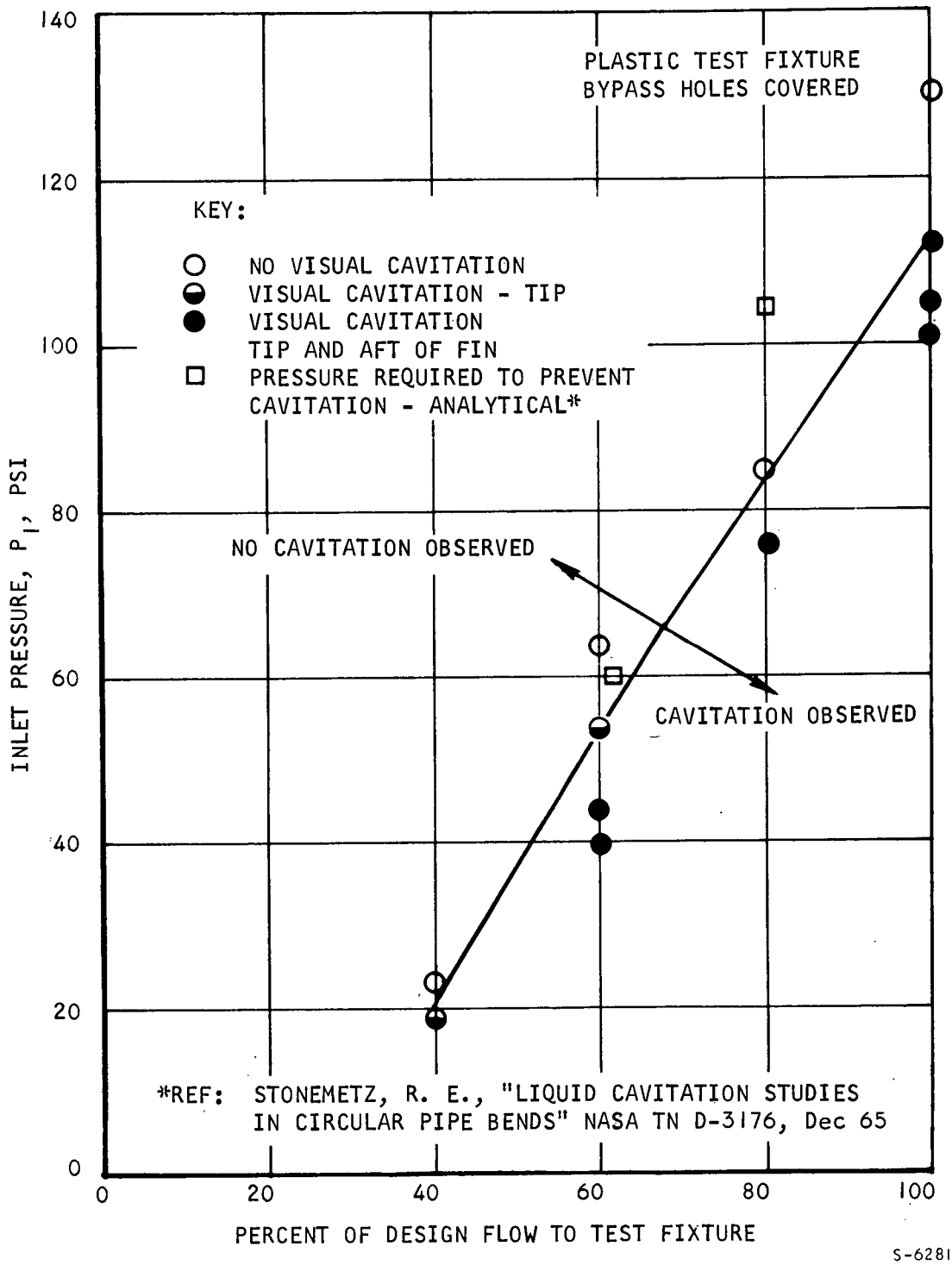

Figure 7-2. Segmented Full-Scale C.L.E. - Results of Cavitation Observations

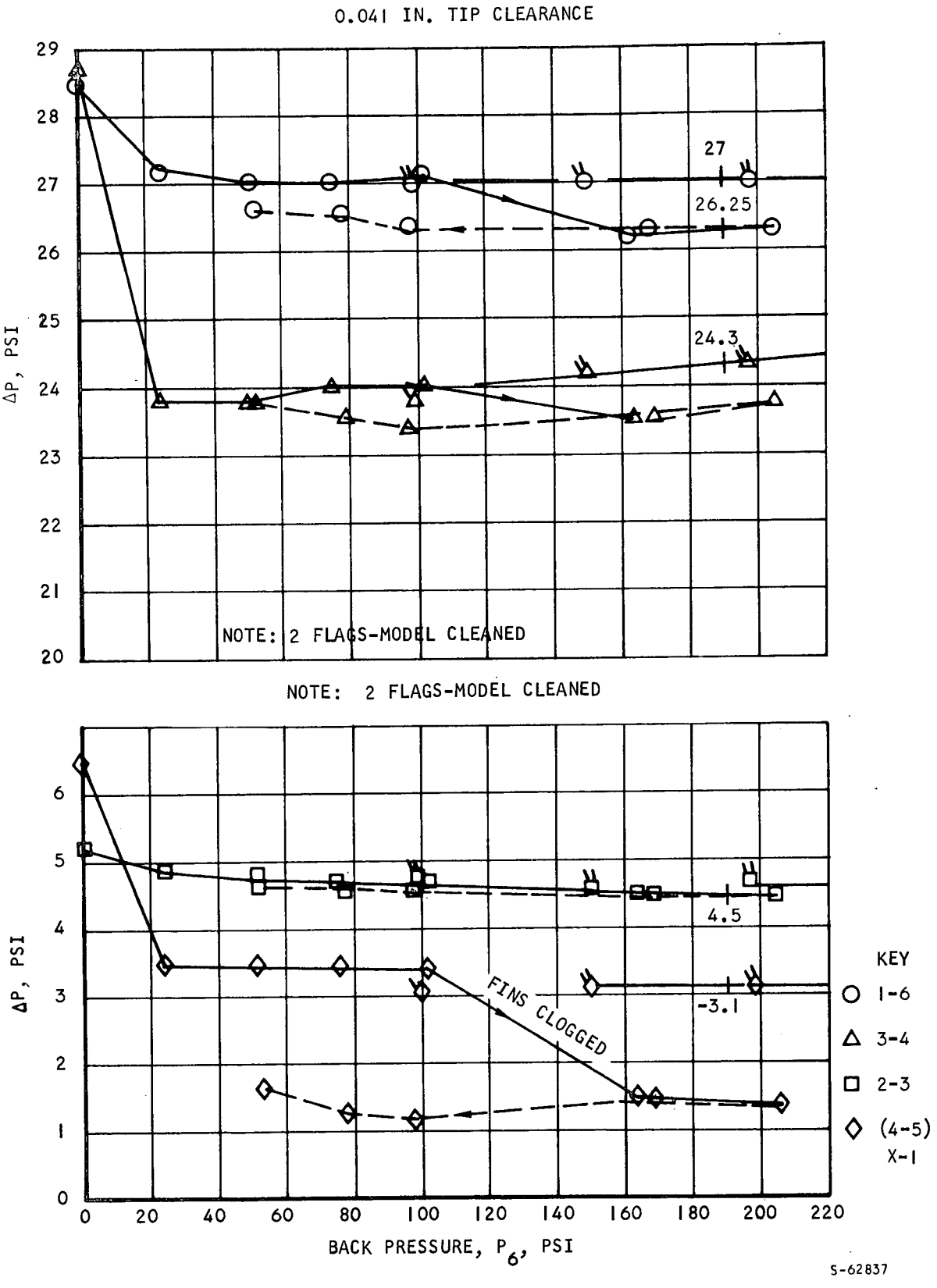

Figure 7-3. Segmented Full-Scale C.L.E. Pressure Drops - 40 Percent Flow, No Bypass

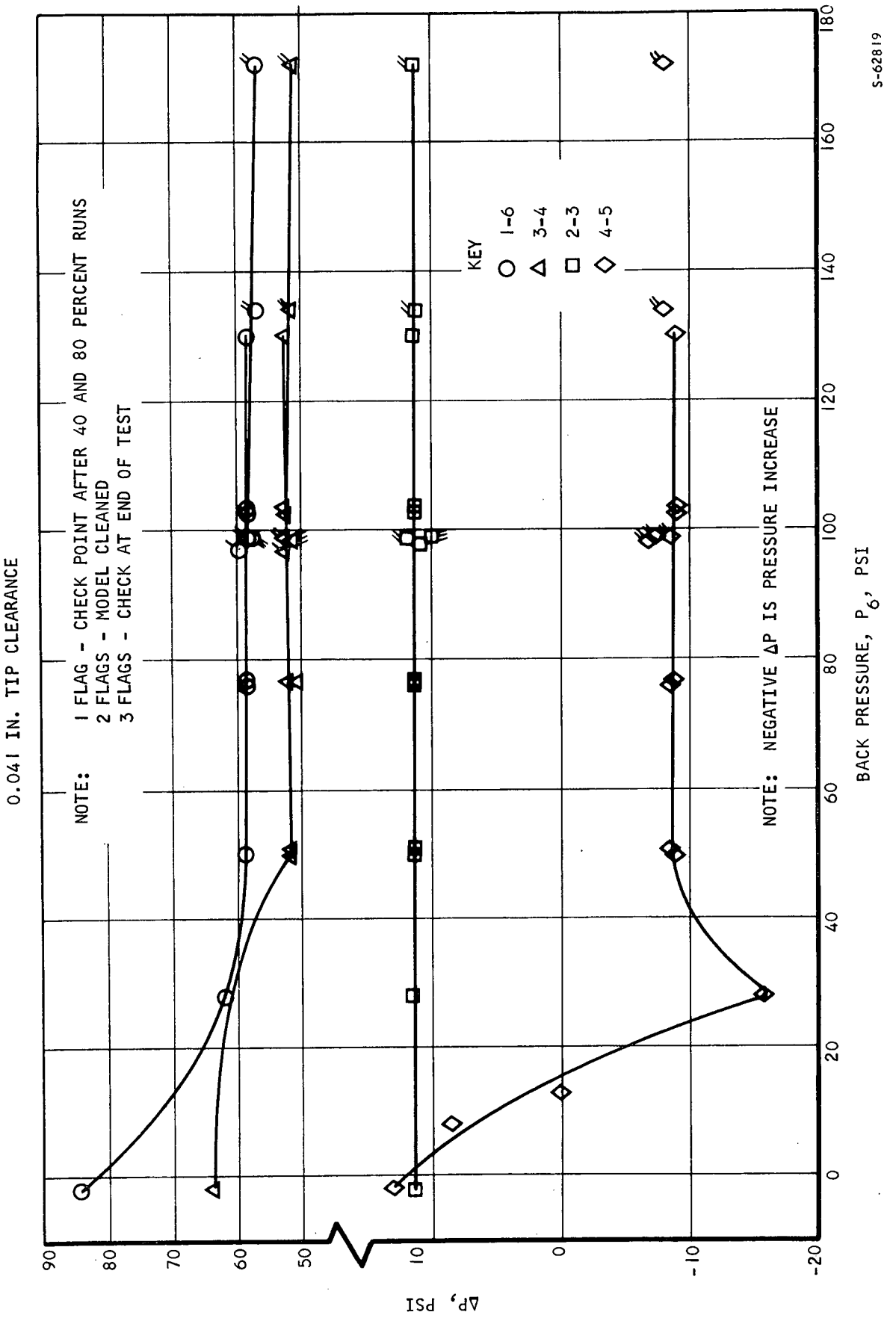

Figure 7-4. Segmented Full-Scale C.L.E. Pressure Drops - 60 Percent Flow, No Bypass

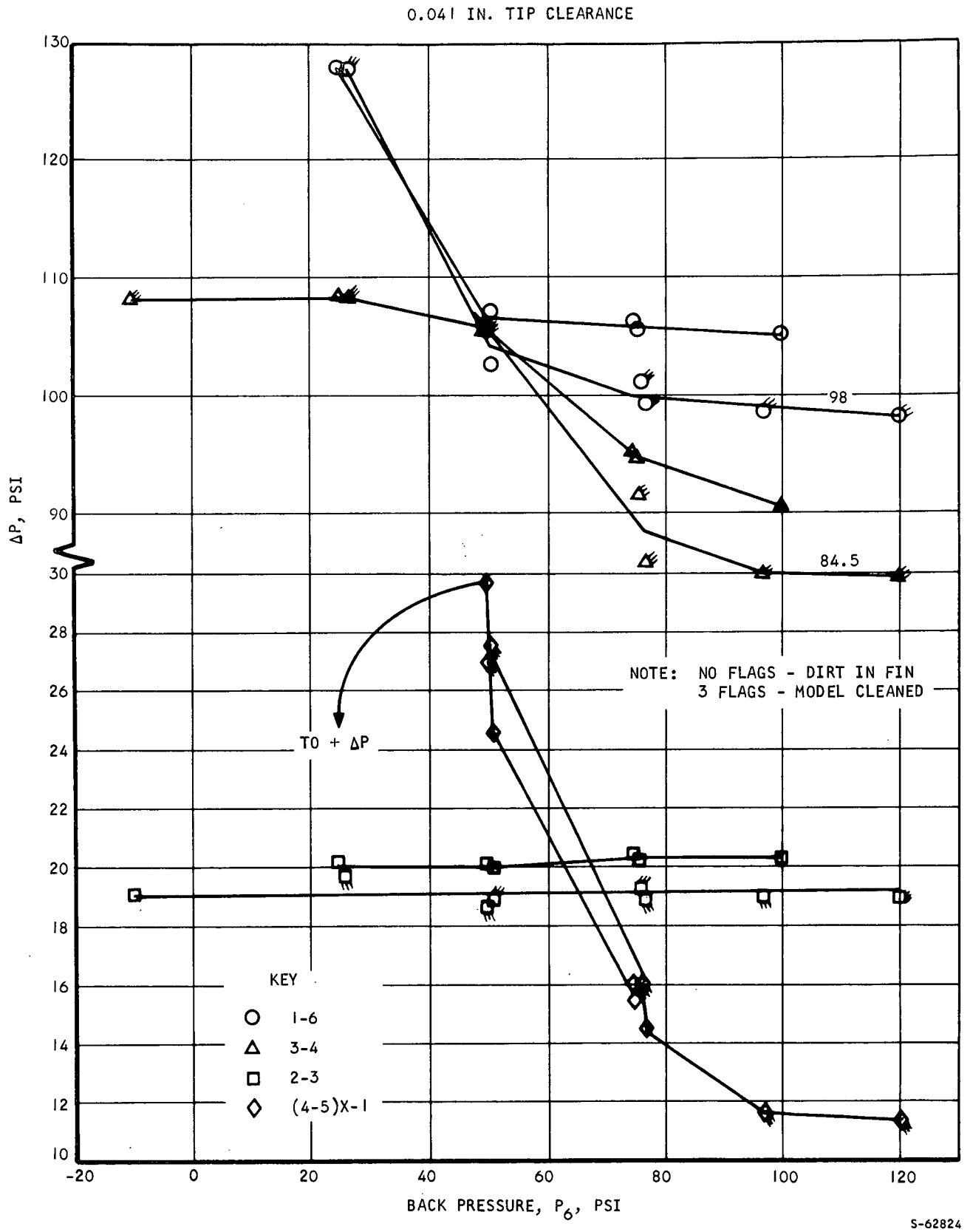

Figure 7-5. Segmented Full-Scale C.L.E. Pressure Drops - 80 Percent Flow, No Bypass

tip flow meter. The effects of cavitation appear to extend to pressures beyond those associated with visual cavitation but significantly below design pressures. Figure 7-6 shows the same data at maximum back pressure, plus additional data taken at intermediate flows and at design inlet pressure, as a function of percent of design flow. The dash line is the calculated relationship of pressure drop and flow based on analysis and measurements of the model geometry. The data correlated reasonably well with the exception of the 4-5 pressure rise.

The foil covering the bypass holes was removed and the model retested as before. These results are shown in Figures 7-7 through 7-10. The 4-5 pressure rise is not shown as that measurement was unstable, possibly due to the influence of the bypass flow on pressure tap No. 5. The data correlated well and indicate 44 percent tip flow based on the 2-3 measurement, and 42 percent based on the 3-4 measurement. It was decided that the pressure drop and flow split were sufficiently close to design to commit hardware based upon this configuration to the full scale AIM fabrication.

7.1.2 Correlation of 10X-Scale Plastic and Segmented Full-Scale Data

The 10X-scale model data configuration No. 6, reported on during the last period, indicated approximately 59 percent tip flow for the design case. The corresponding measured value from the segmented test was 44 percent, based on the 2-3 pressure tap. Since pressure drop is proportional to $(\text{flow/flow area})^2$, the following scaling factor was derived for conversion of the 10X-scale pressure drops to full scale.

$$(\Delta P)_{F.S.} = \frac{\Delta P_{10X}\left[(W/A)_{F.S.} \Big/ (W/A)_{10X}\right]^2}{27.7} \qquad (7\text{-}1)$$

$$= \frac{(\Delta P)_{10X}\left[(18.3/1.61) \Big/ \{102/(8.8 \times 10)\}\right]^2}{27.7}$$

$$= 3.48\ (\Delta P)_{10X}\ \text{psi, where } (\Delta P)_{10X} \text{ is in inches of water.}$$

Use of Equation (7-1) and the 10X-scale data predicts an overall pressure drop of 66 psi for a no-bypass at 80 percent of design flow, and 47 psi with bypass at 100 percent of design flow. The corresponding measured values from the segment model test are 98 psi and 66 psi respectively. The segmented model was subsequently inspected to determine if there were geometry differences that might explain the difference in test results between the segmented model and the 10X-scale model. It was found that the tip gap was approximately 0.041 in. rather than the design value of 0.050 in.

An analysis was made to investigate if this discrepancy could explain the differences in the test data. The following schematic is a simplification of the flow route through the model where it is assumed that the pressure drop across both restrictions is equal.

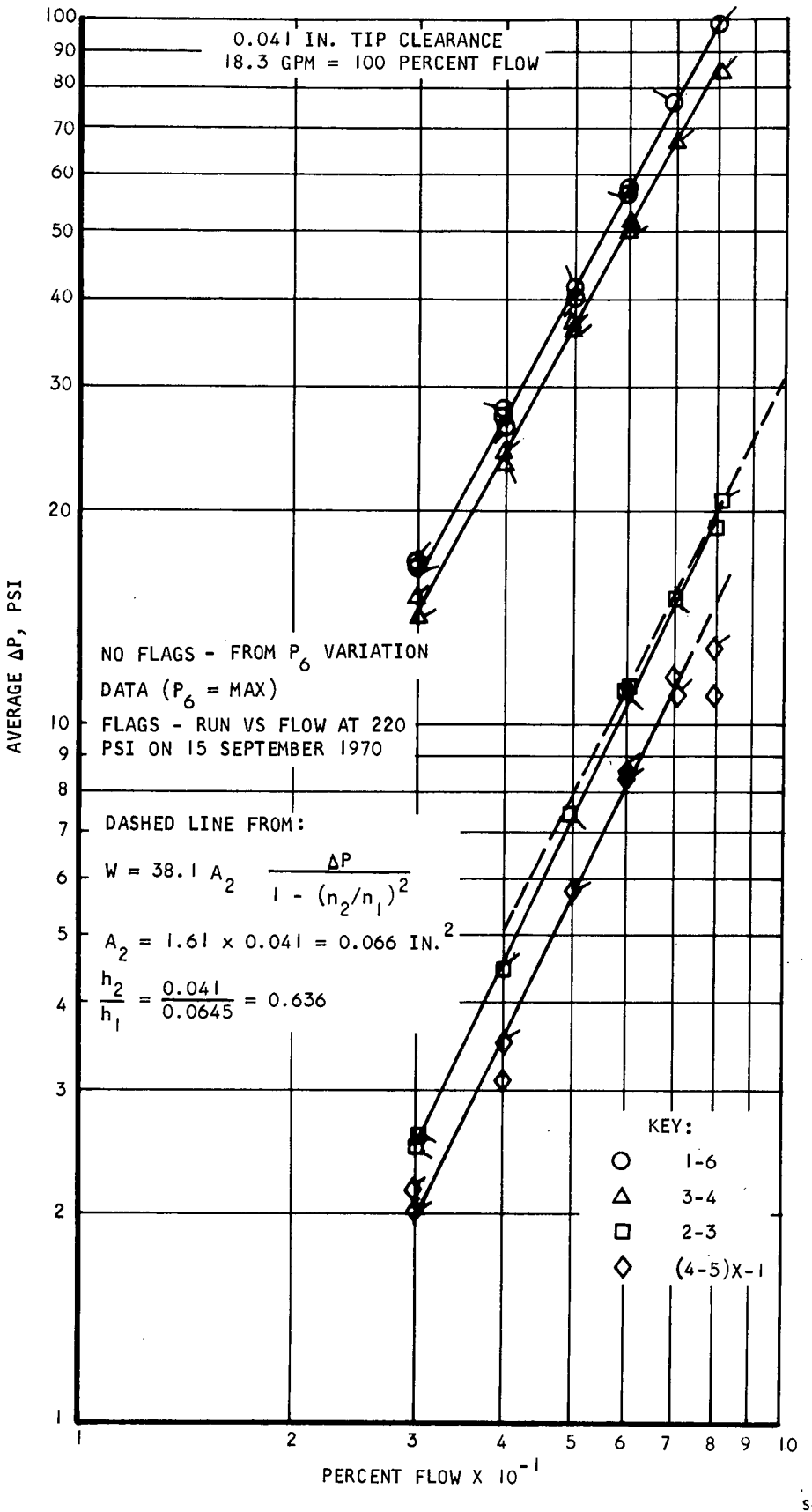

Figure 7-6. Segmented Full-Scale C.L.E. Pressure Drops - X-Plot at Maximum P_6, No Bypass

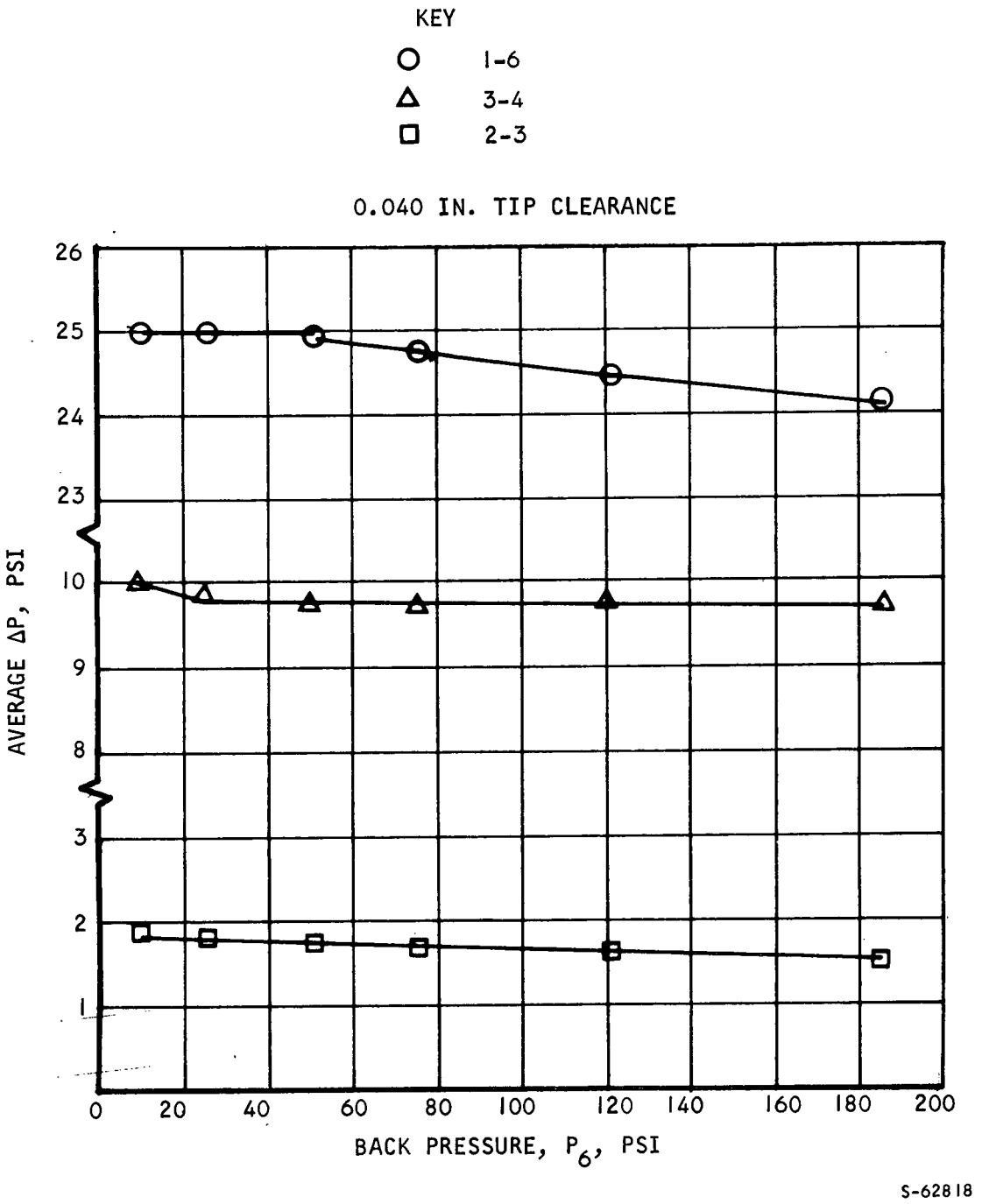

Figure 7-7. Segmented Full-Scale C.L.E. Pressure Drops - 60 Percent Flow, With Bypass

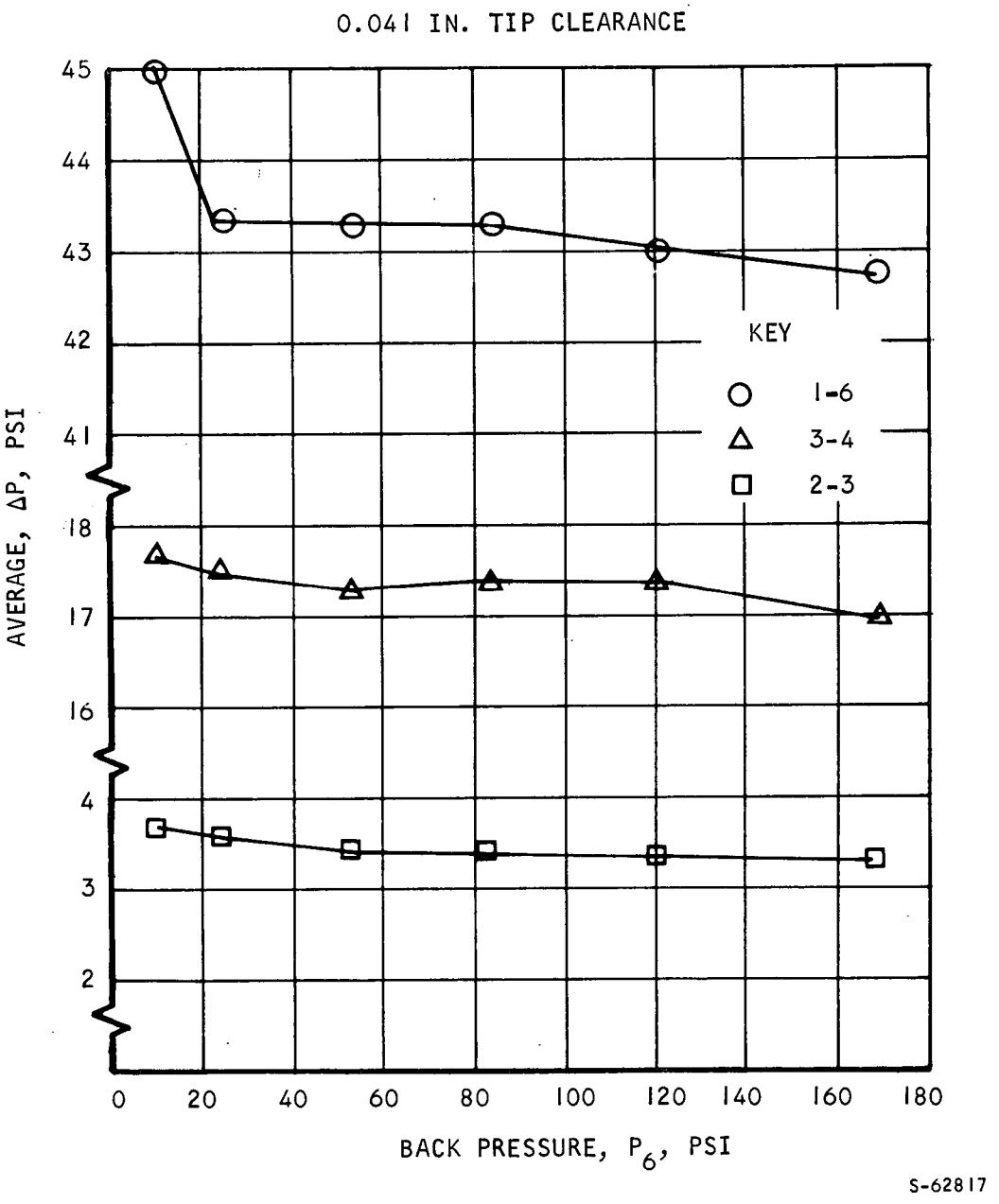

Figure 7-8. Segmented Full-Scale C.L.E. Pressure Drops - 80 Percent Flow, With Bypass

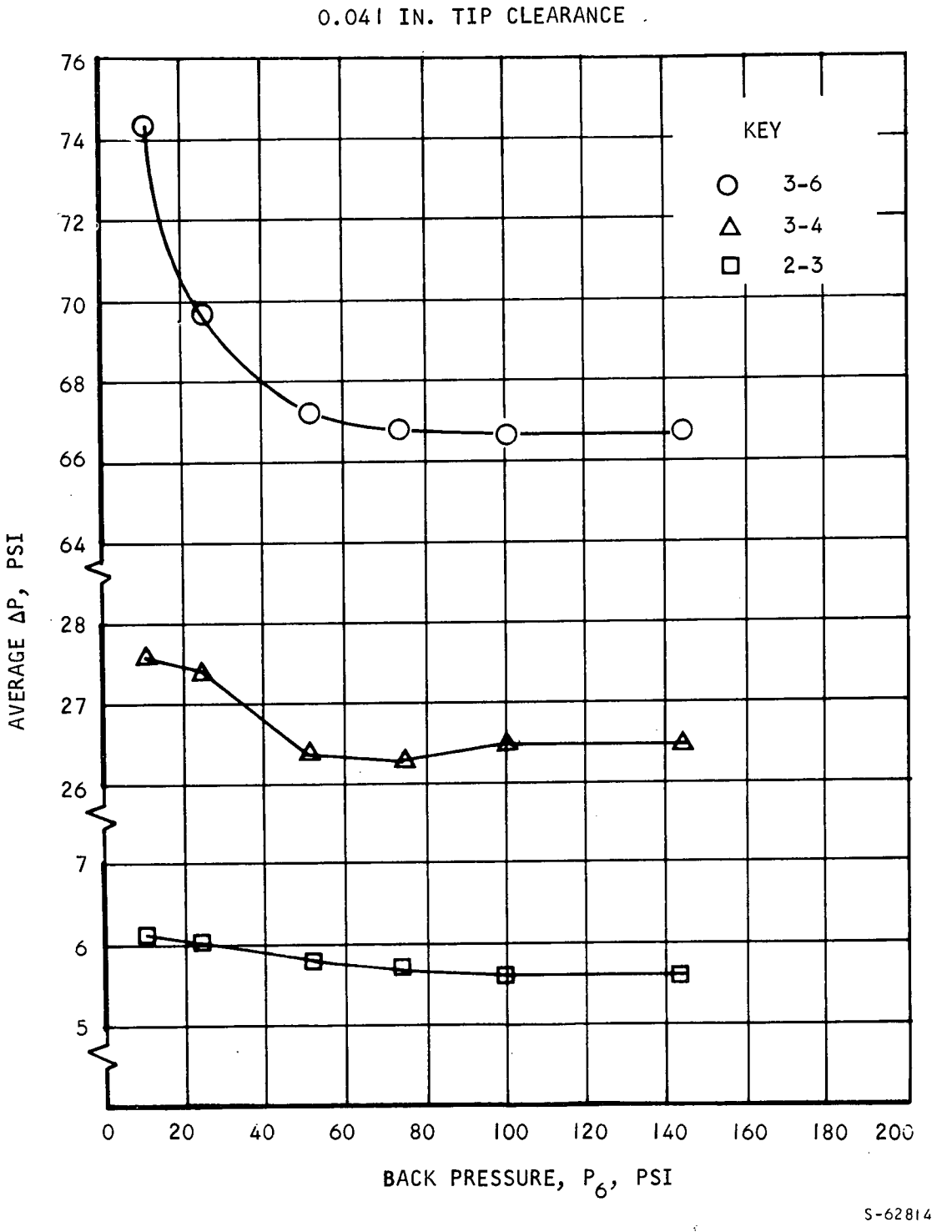

Figure 7-9. Segmented Full-Scale C.L.E. Pressure Drops - 100 Percent Flow, With Bypass

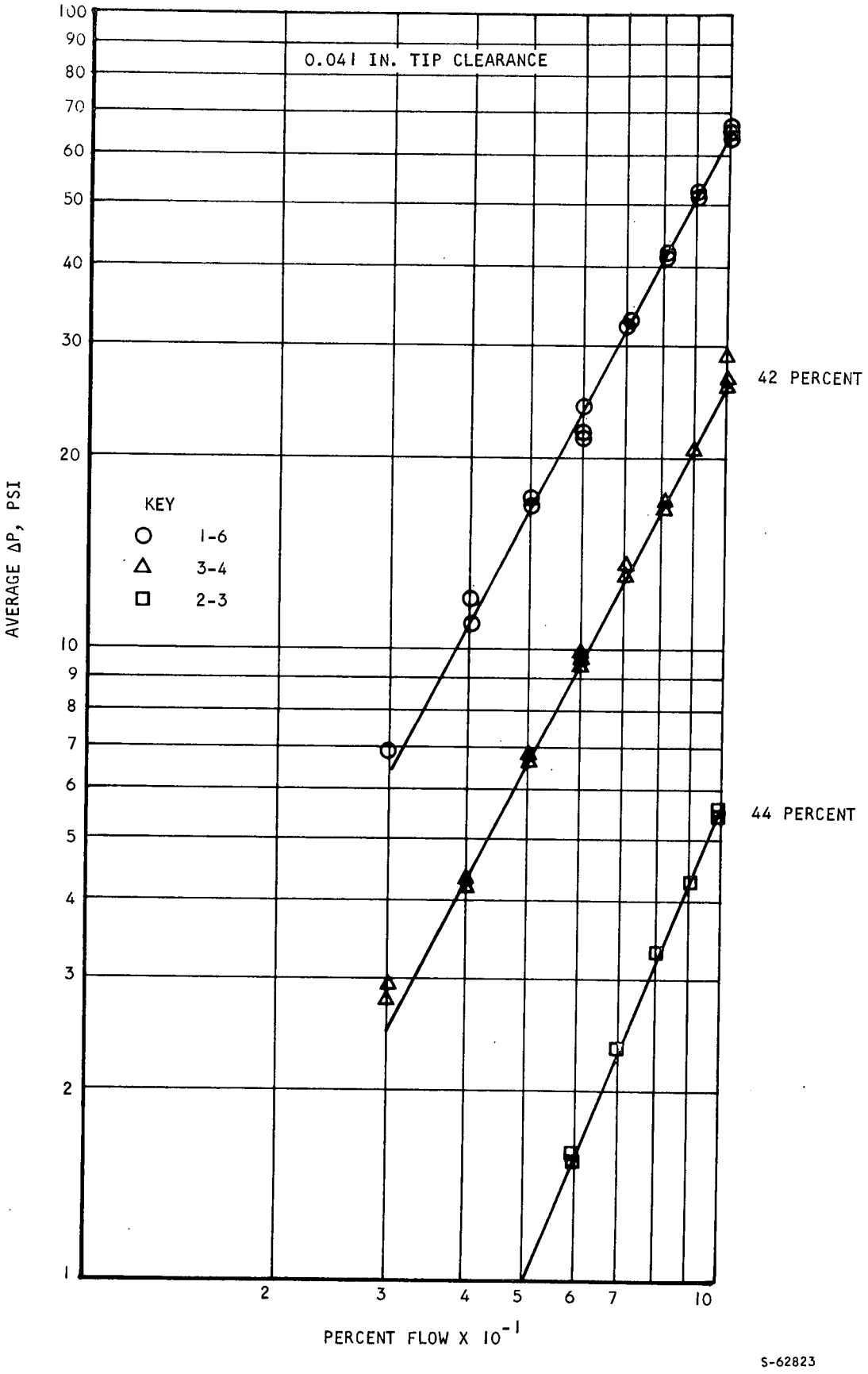

Figure 7-10. Segmented Full-Scale C.L.E. Pressure Drops - With Bypass

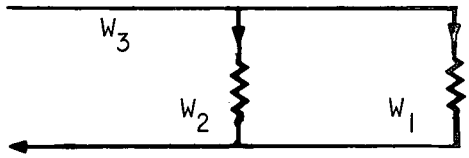

For the flow schematic shown on the above sketch, it can be shown that:

$$\frac{W_1}{W_3} = \frac{1}{1 + K \frac{A_2}{A_1}} \tag{7-2}$$

where A_1 and A_2 are the effective flow areas associated with the two flow paths, and K is defined by

$$K = \frac{A_1}{A_2}\left(\frac{W_3}{W_1} - 1\right) \tag{7-3}$$

Based upon the 10X-scale model for configuration 6

$$K = \frac{8.8 \times 0.5}{6 \times \pi/4\ (0.7)^2}\left(\frac{1}{0.53} - 1\right) = 1.325 \tag{7-4}$$

The area of the 0.1-in.-wide slots located on every third hole was neglected, as that bypass area should have a poor discharge coefficient.

From Equations (7-2) and (7-4) and the segmented model geometry

$$\frac{W_1}{W_3} = \frac{1}{1 + 1.325\ \frac{11 \times \pi/4\ (0.0713)^2}{1.61 \times 0.041}} = 0.53 \tag{7-5}$$

The measured value is 0.44.

Based upon the same analytical model as described above

$$(\Delta P)_{F.S.} = (\Delta P)_{10X}\left[\frac{1 + K\,(A_2/A_1)_{10X}}{1 + K\,(A_2/A_1)_{F.S}}\right]^2 \frac{(W_3)^2_{FS}}{(W_3)^2_{10X}} \frac{(A_1)^2_{10X}}{(A_1)^2_{FS}} \tag{7-6}$$

The factor K is from Equation (7-3) with the values based upon 10X-scale model data from Equation (7-4). Equation (7-6) results in predicted values for the overall pressure drop with bypass and without bypass ($A_2 = 0$) of 54 psi and 36 psi, respectively, compared to the measured values of 66 psi and 41 psi, respectively. The bypass case was evaluated at 100 percent of design flow and the no-bypass case at 50 percent of design flow.

A similar calculation was made to predict the performance of the full-scale, full-round slotted bypass design based upon the 10X-scale model data, configuration 5. These calculations resulted in a predicted overall pressure drop of 77 psi compared to a measured pressure drop of 81 psi at 100 percent design flow. The predicted tip flow was 82 percent compared to the estimated value of 75 percent.

7.1.3 Additional Segmented Full-Scale Model Tests

The above analytical correlation of data tends to corroborate the results of both the segmented full-scale model and the 10X-scale model tests. To verify these results, the segmented full-scale model was disassembled and reworked to attain the design tip leading edge gap of 0.050 in. Due to the rework, the precise relationship of the flow divider in the 2-3 pressure taps could not be held the same as in prior tests, and therefore the 0.003-in. foil was included in the model as before for a flow calibration. These test results are shown in Figures 7-11 through 7-18.

The performance for this configuration, which should be the same as the new full-scale, full-round cowl leading edge, was predicted in two ways. The first, using the 10X-scale model data, resulted in a tip flow of 58 percent and an overall pressure drop of 44 psi at 100 percent design flow. The second, using the segmented full-scale model data, resulted in a tip flow of 49 percent and an overall pressure drop of 55 psi at 100 percent design flow. Figure 7-18 shows an overall pressure drop of 52 psi and a tip flow of 52 percent.

Since the precise location of the flow divider in the cowl leading edge has been a problem, it was decided to rework the flow divider in the segmented model to a tip spacing of 0.060 in. to further explore the sensitivity of the data to mislocation. These test results are shown in Figures 7-19 through 7-26. These data do not seem to correlate well with the data taken with the 0.041-in. and 0.050-in. tip spacing, but do still yield an acceptable flow split and pressure drop. It was therefore concluded that this flow divider configuration should be acceptable with a tip spacing of 0.050 ±0.010 in.

7.1.4 Full-Scale Test

A full-round, full-scale cowl leading edge assembly was tested to verify the above conclusion. The tip spacing varied from 0.054 in. to 0.058 in. The test results are shown in Figures 7-27 and 7-28. It was not possible to measure the flow split with the available test setup, and only the overall pressure drop was recorded. After testing it was noted that some small shavings of the test fixture O-ring had been trapped in the cowl leading edge tip. This was caused by improper O-ring installation during assembly of the test fixture, and it was concluded that the overall pressure drop would have been (for a clean tip) somewhat lower than the average measured value of approximately 60 psi at design flow. It was further concluded that the assembly was acceptable and that the second cowl leading edge would not be tested but accepted on the basis of inspection.

A summary of leading edge model test results is shown in Table 7-I.

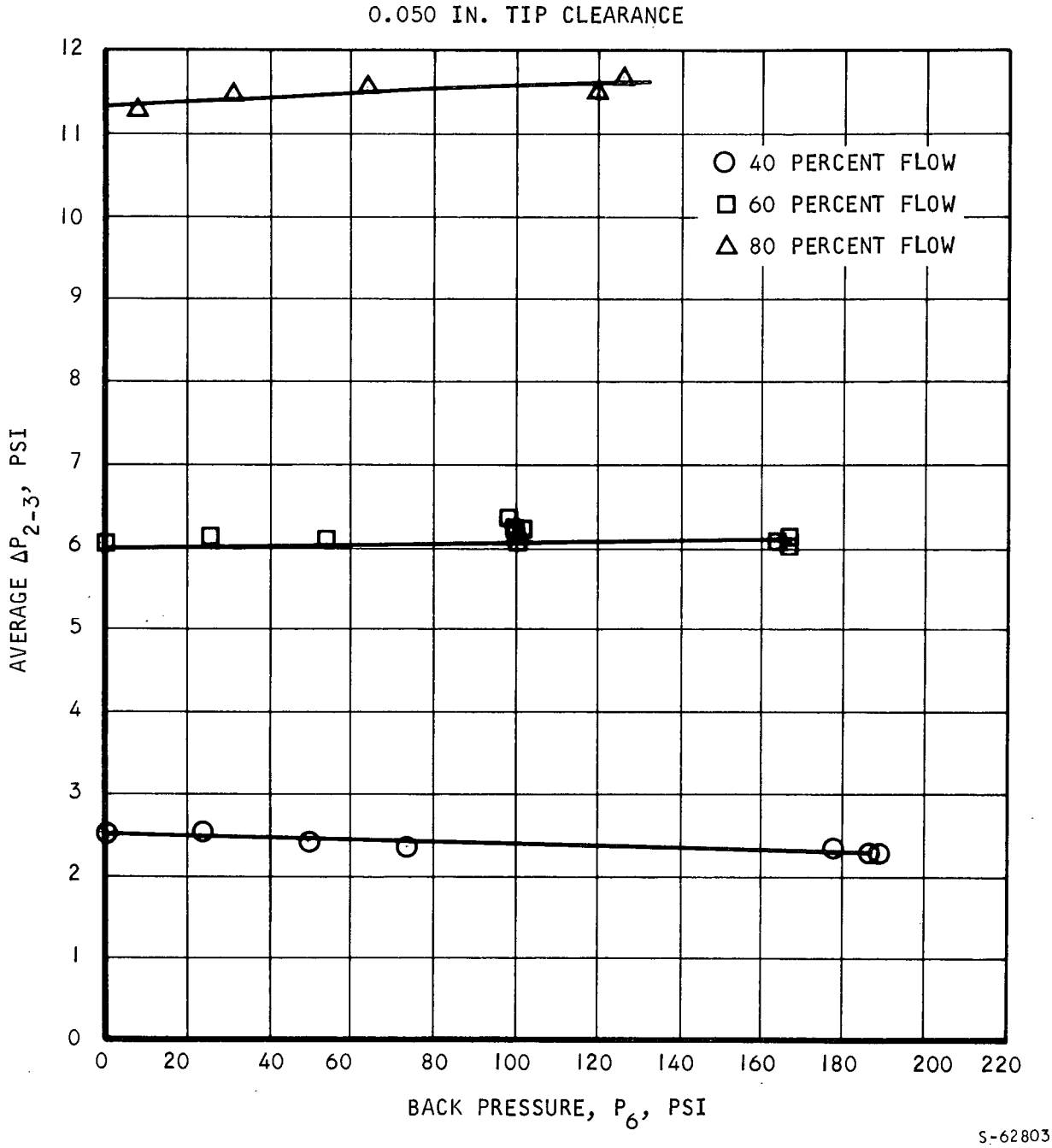

Figure 7-11. Segmented Full-Scale C.L.E. Pressure Drops - No Bypass, Flowmeter ΔP_{2-3} Versus Back Pressure

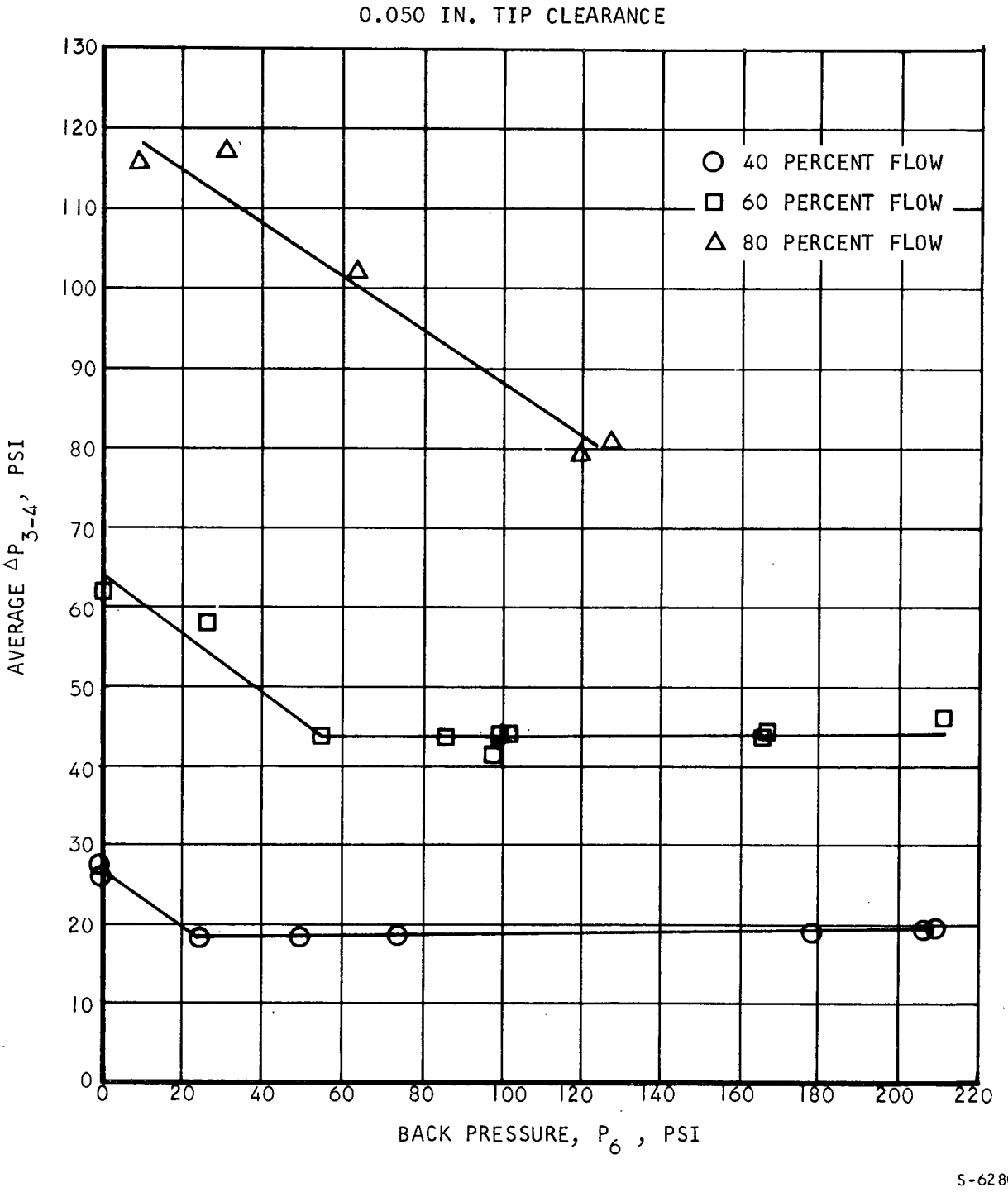

Figure 7-12. Segmented Full-Scale C.L.E. Pressure Drops - No Bypass, Tip ΔP_{3-4} Versus Back Pressure.

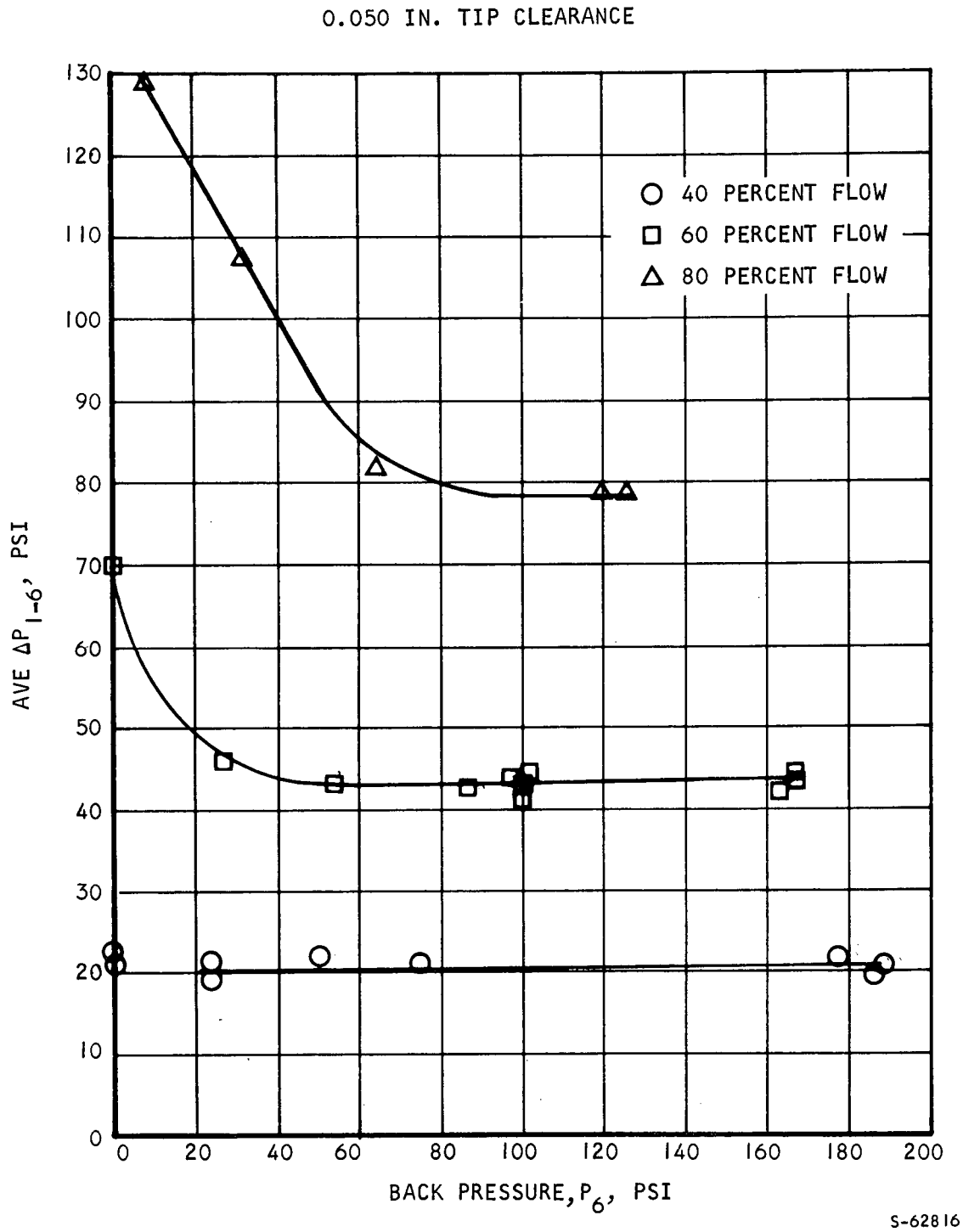

Figure 7-13. Segmented Full-Scale C.L.E. Pressure Drops - No Bypass, Overall ΔP_{1-6} Versus Back Pressure

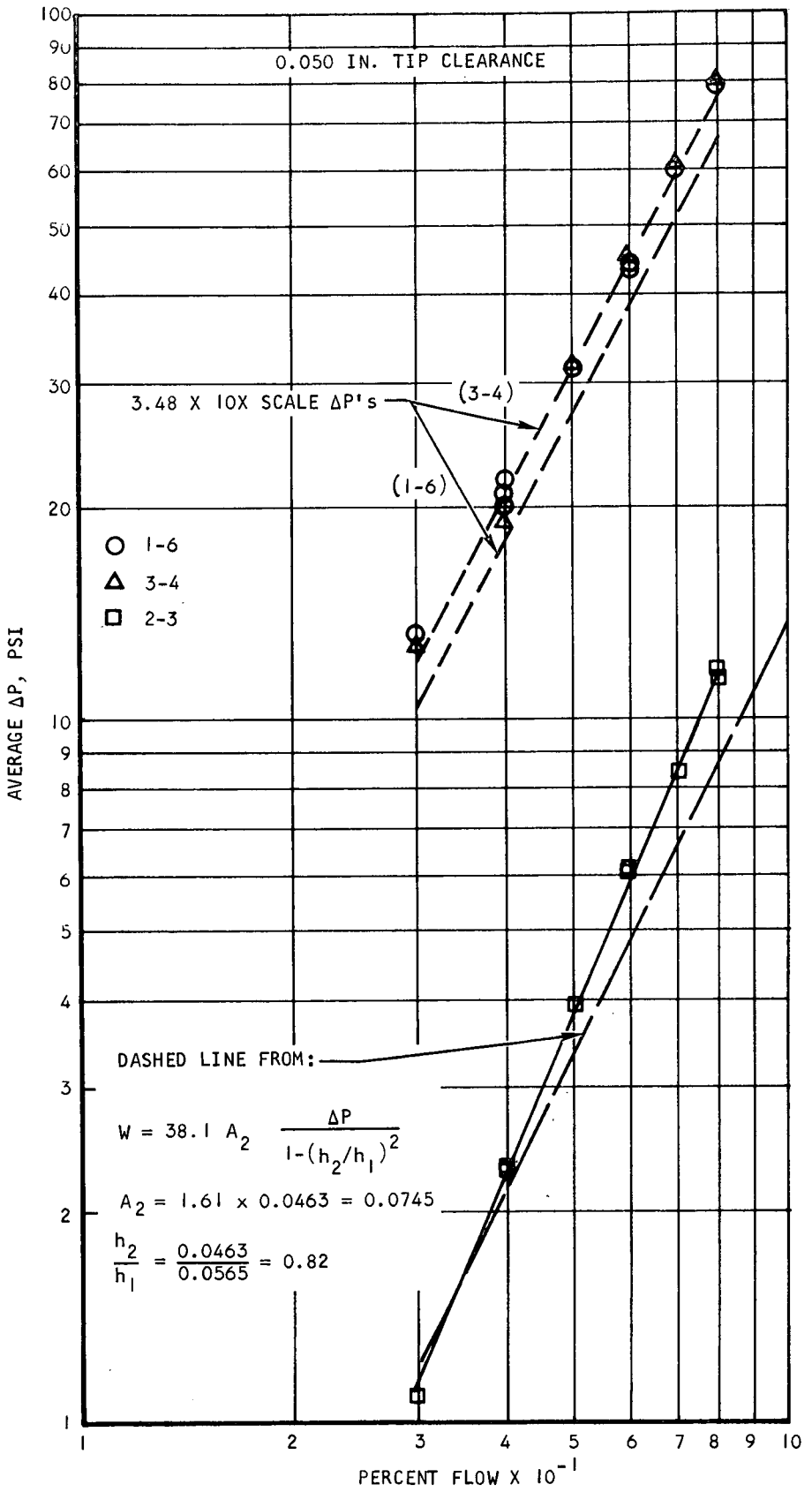

Figure 7-14. Segmented Full-Scale C.L.E. Pressure Drops - No Bypass, Maximum P_6

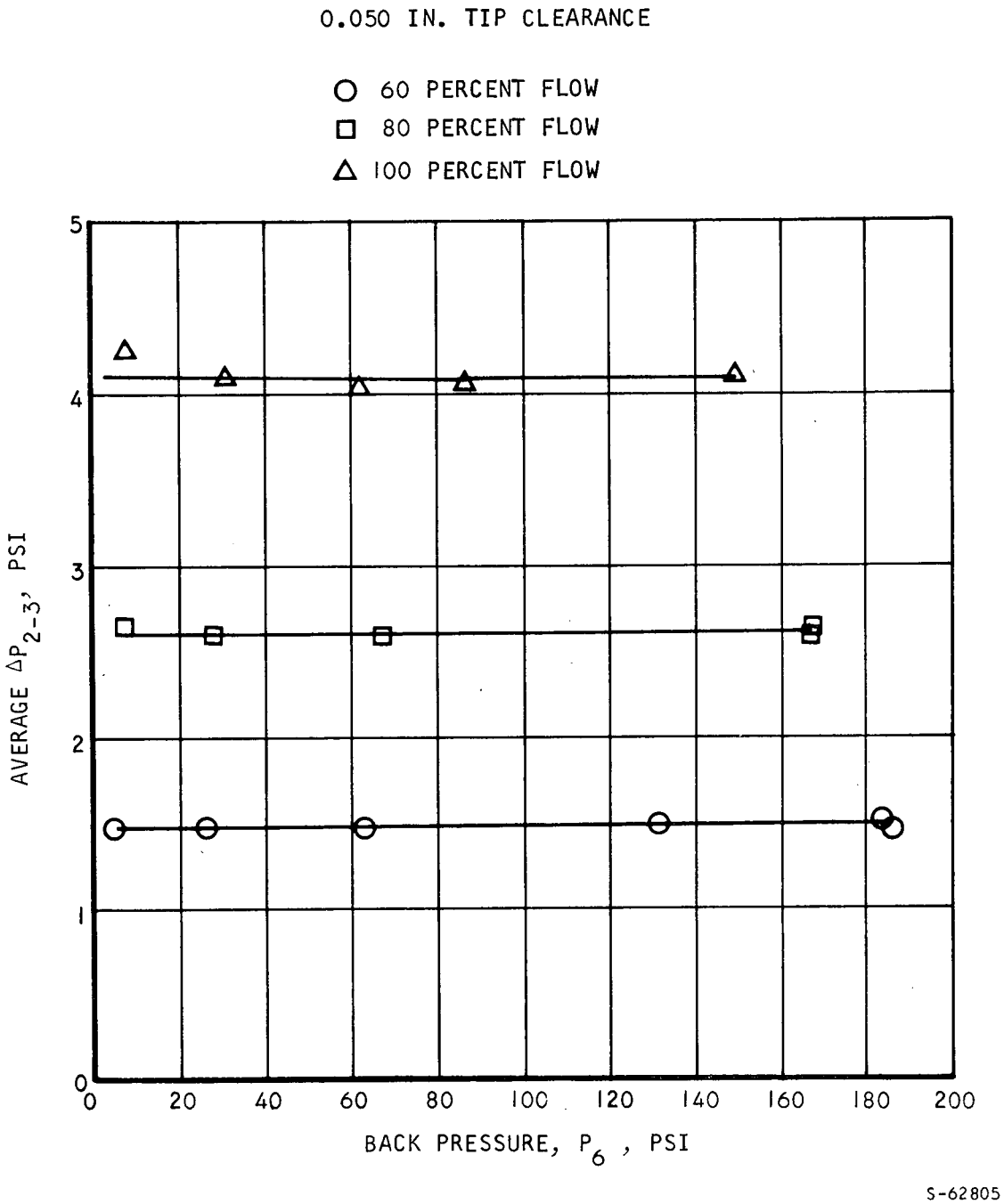

Figure 7-15. Segmented Full-Scale C.L.E. Pressure Drops - With Bypass, Flowmeter ΔP_{2-3} Versus Back Pressure

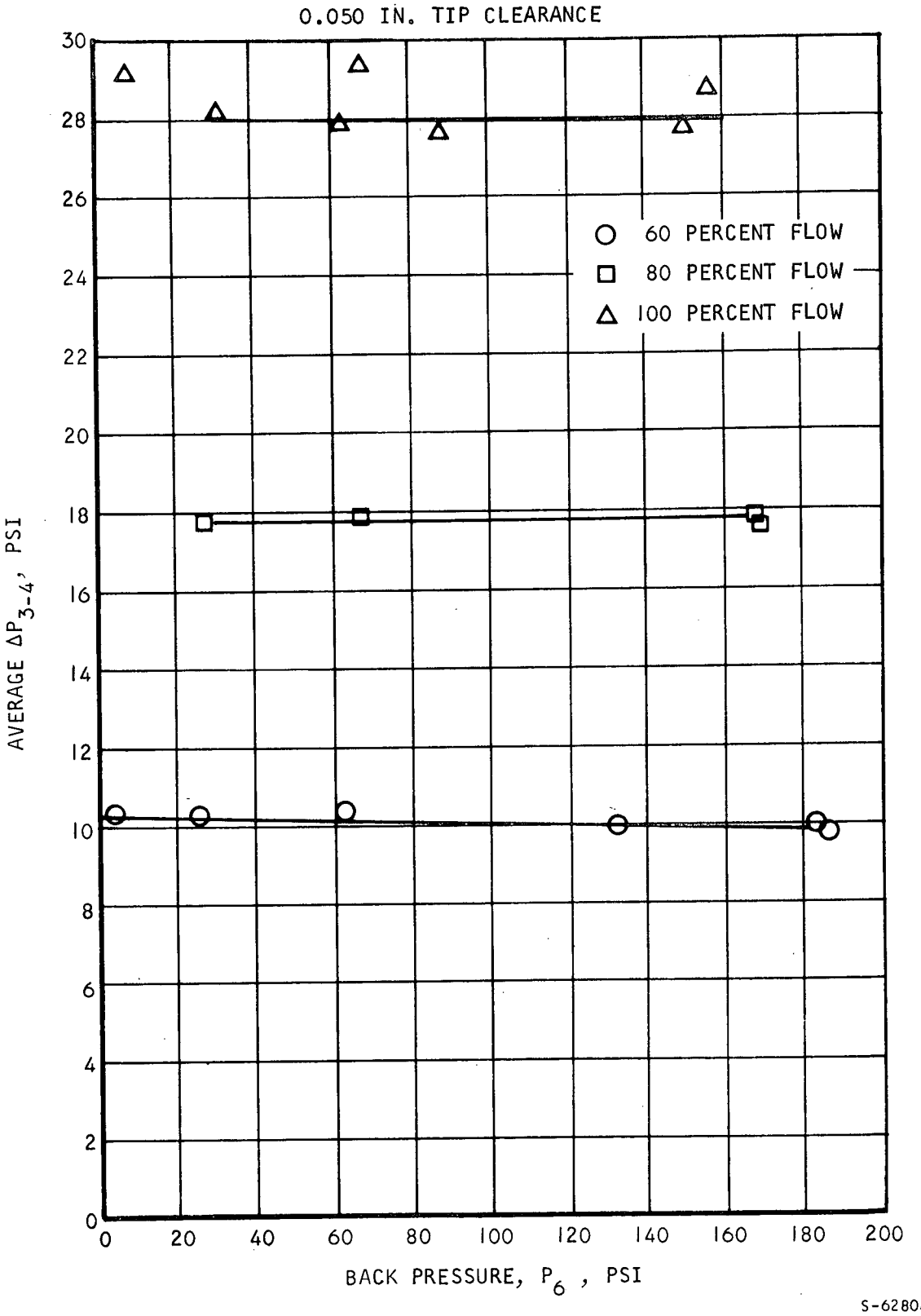

Figure 7-16. Segmented Full-Scale C.L.E. Pressure Drops - With Bypass, Tip ΔP_{3-4} Versus Back Pressure

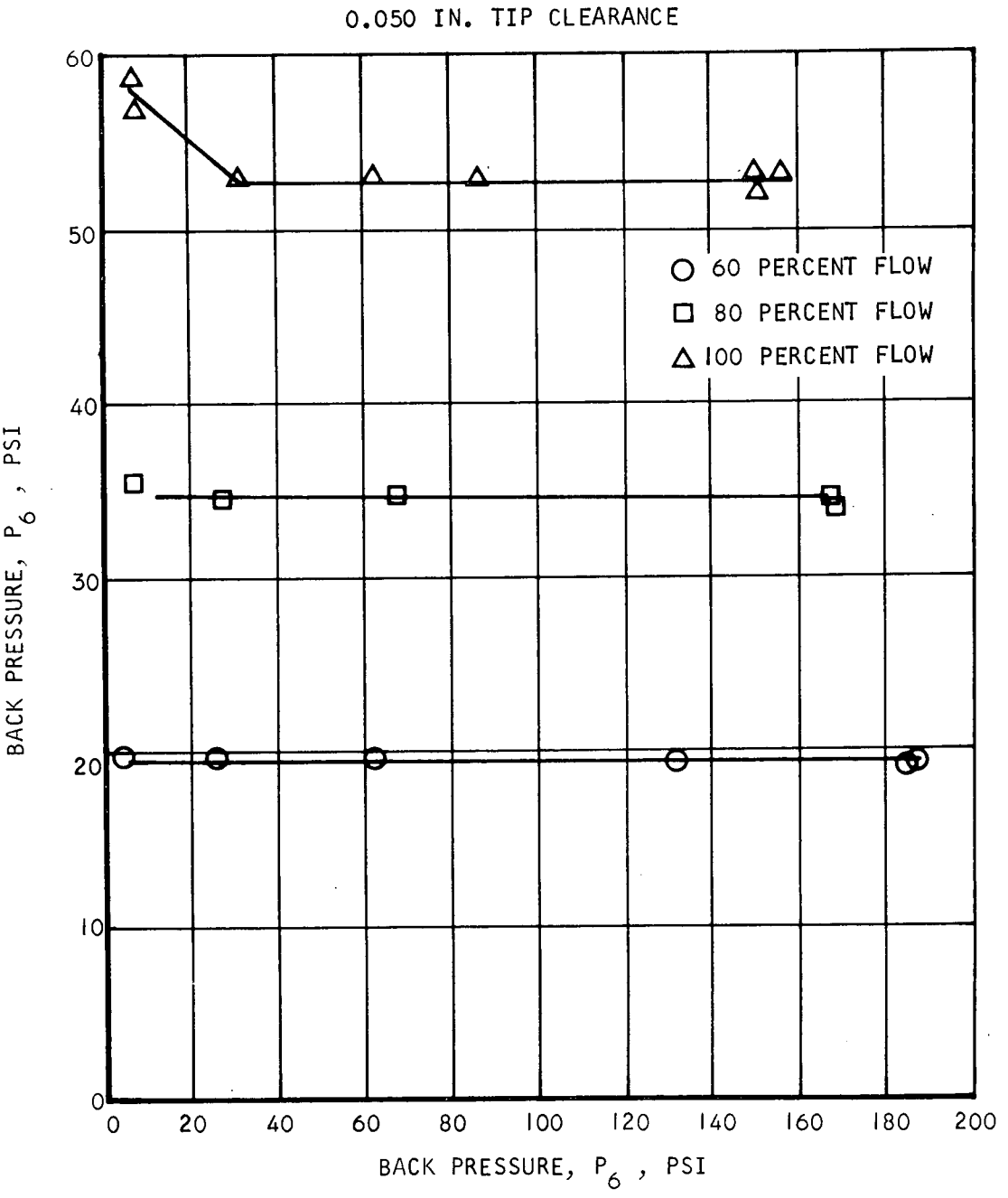

Figure 7-17. Segmented Full-Scale C.L.E. Pressure Drops - With Bypass, Overall ΔP_{1-6} Versus Back Pressure Pressure

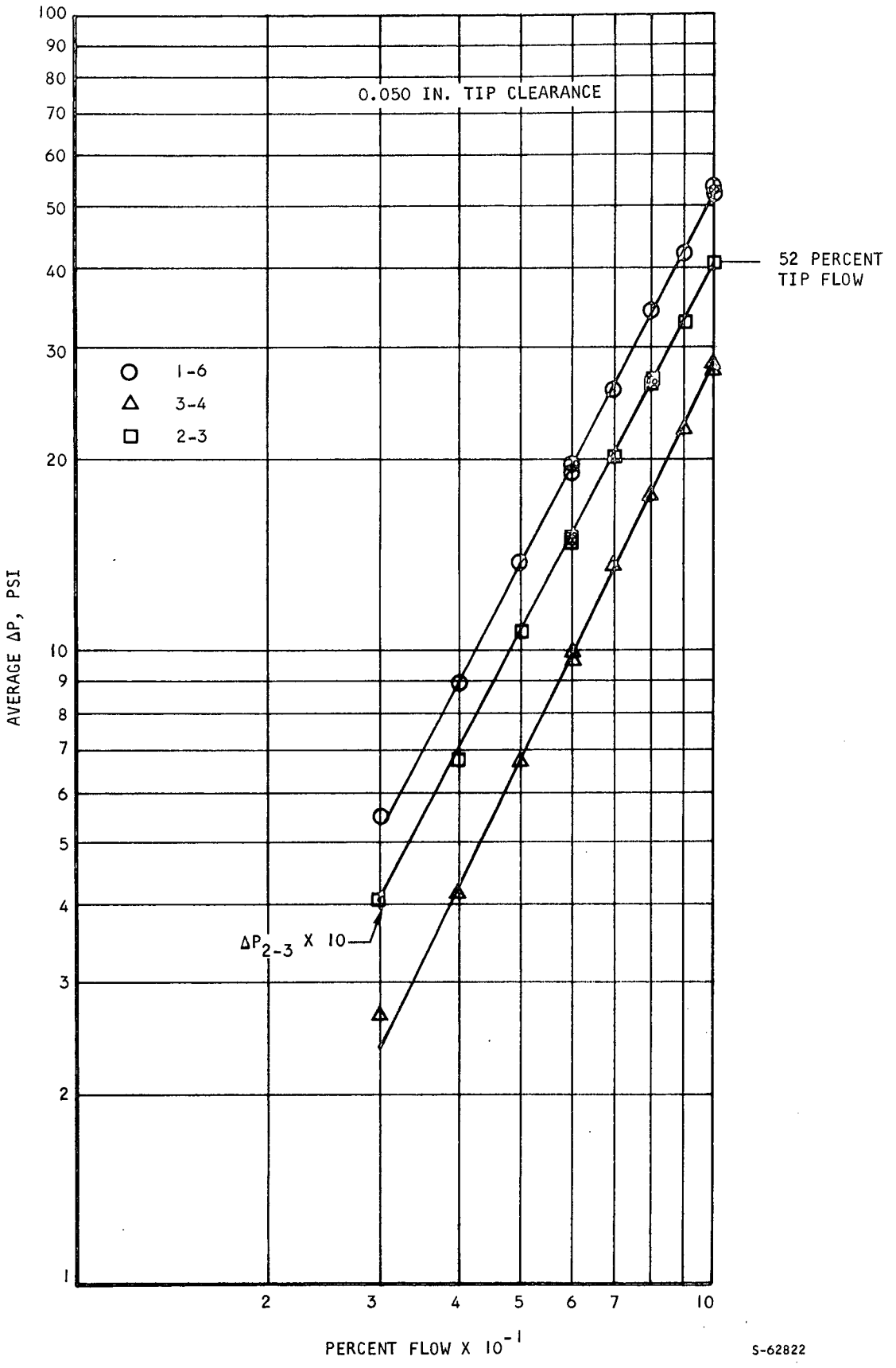

Figure 7-18. Segmented Full-Scale C.L.E. Pressure Drops - With Bypass, Maximum P_6

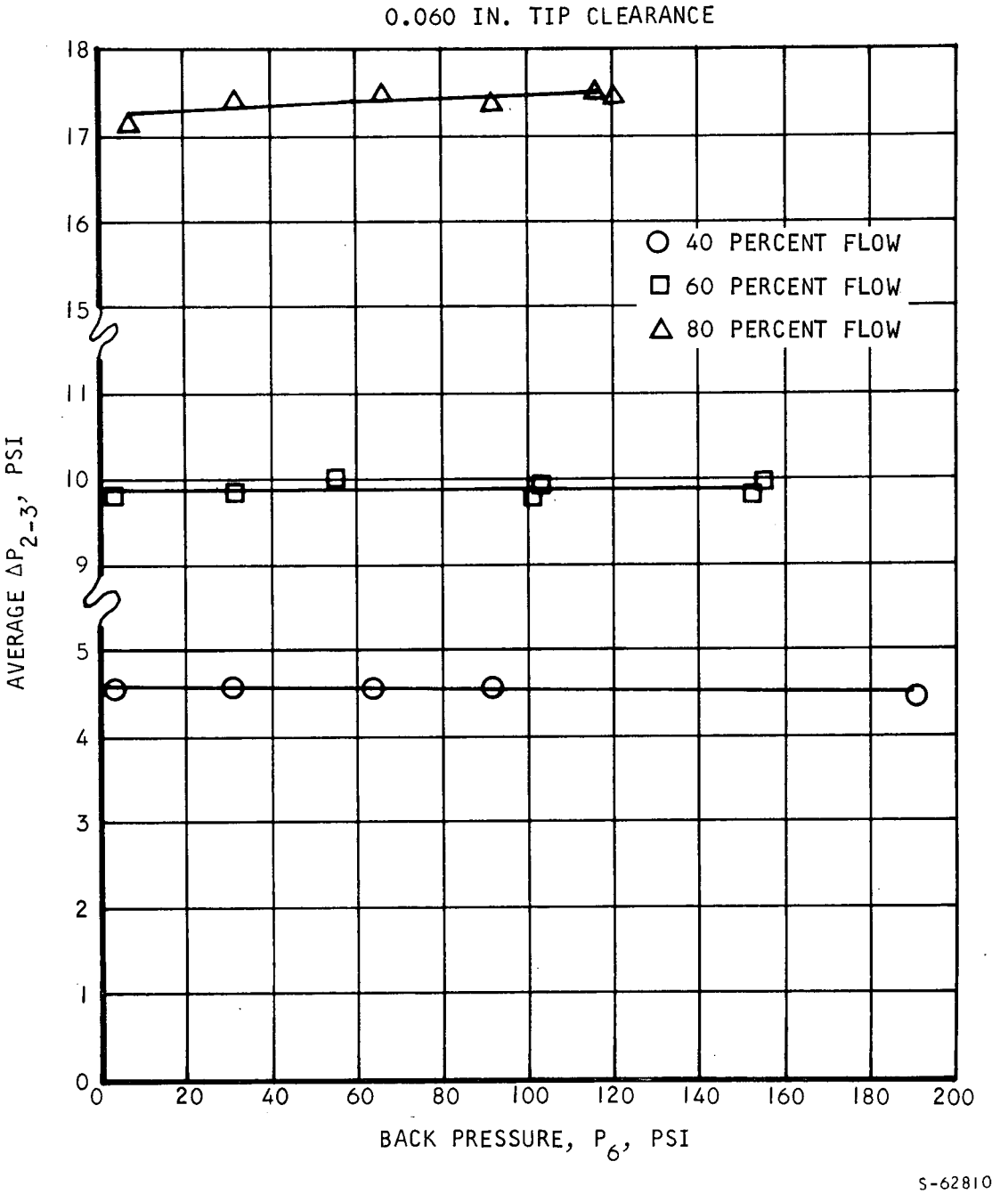

Figure 7-19. Segmented Full-Scale C.L.E. Pressure Drops - No Bypass, Flowmeter ΔP_{2-3} Versus Back Pressure

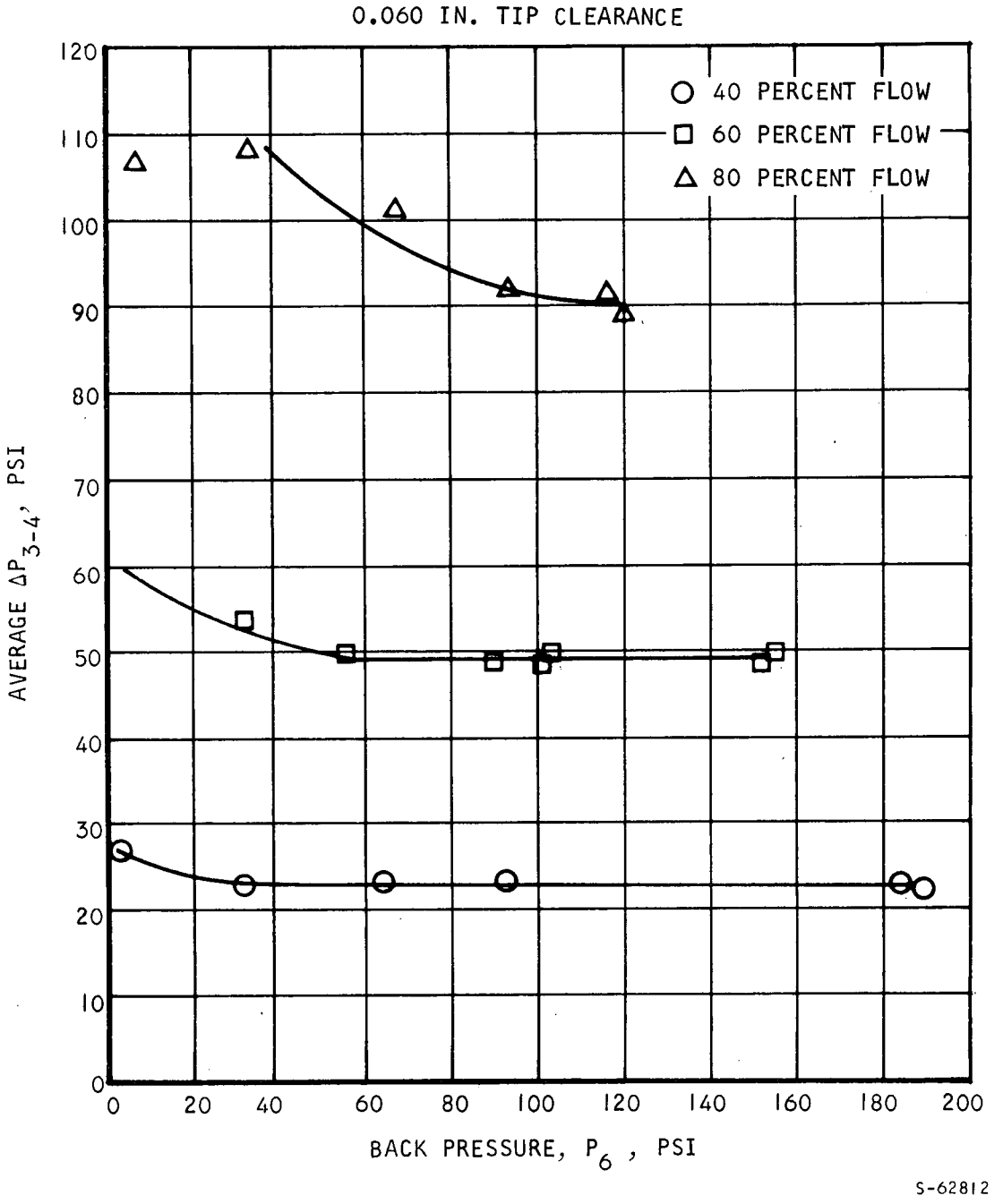

Figure 7-20. Segmented Full-Scale C.L.E. Pressure Drops - No Bypass, Tip ΔP_{3-4} Versus Back Pressure

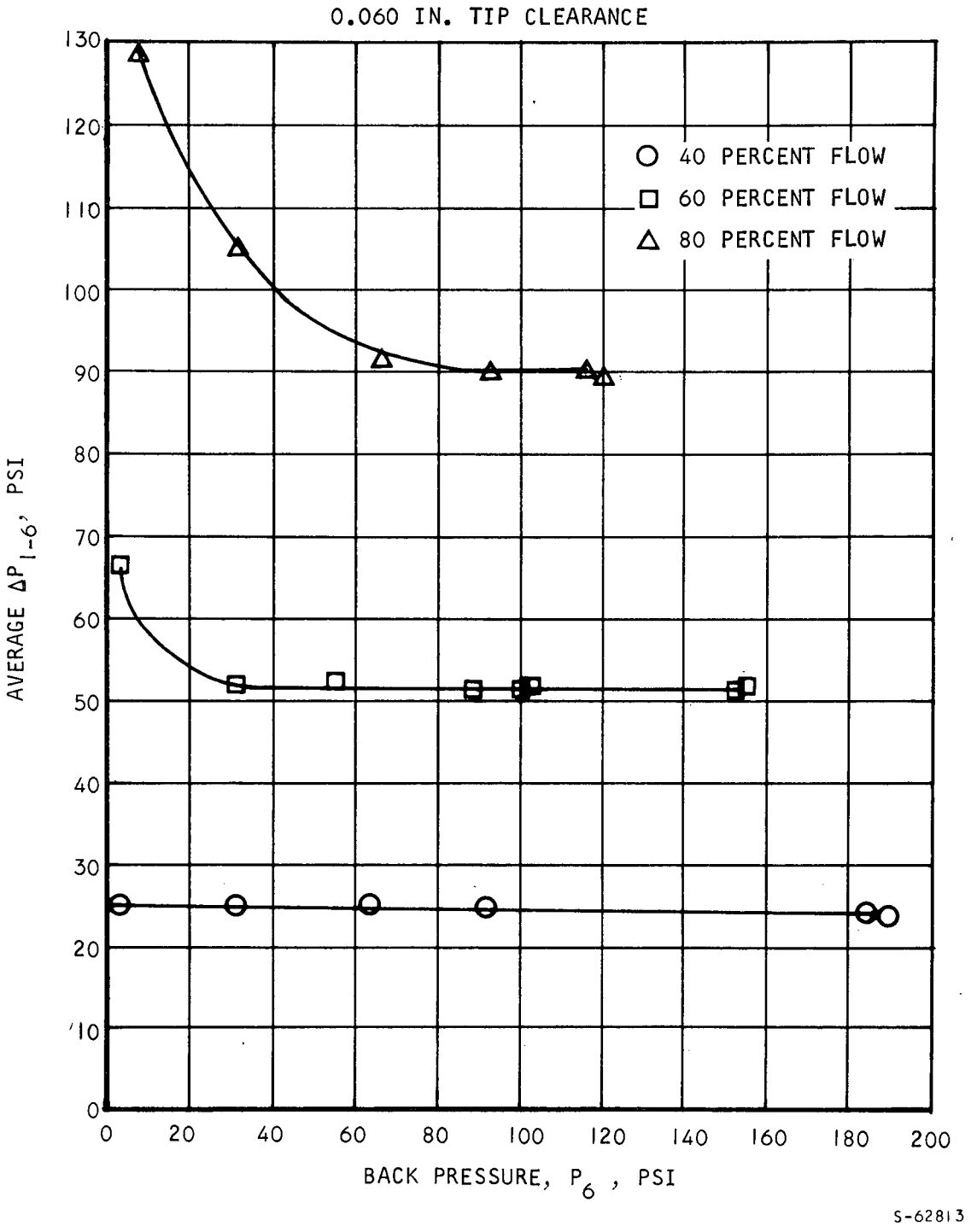

Figure 7-21. Segmented Full-Scale C.L.E. Pressure Drops - No Bypass, Overall ΔP_{1-6} Versus Back Pressure

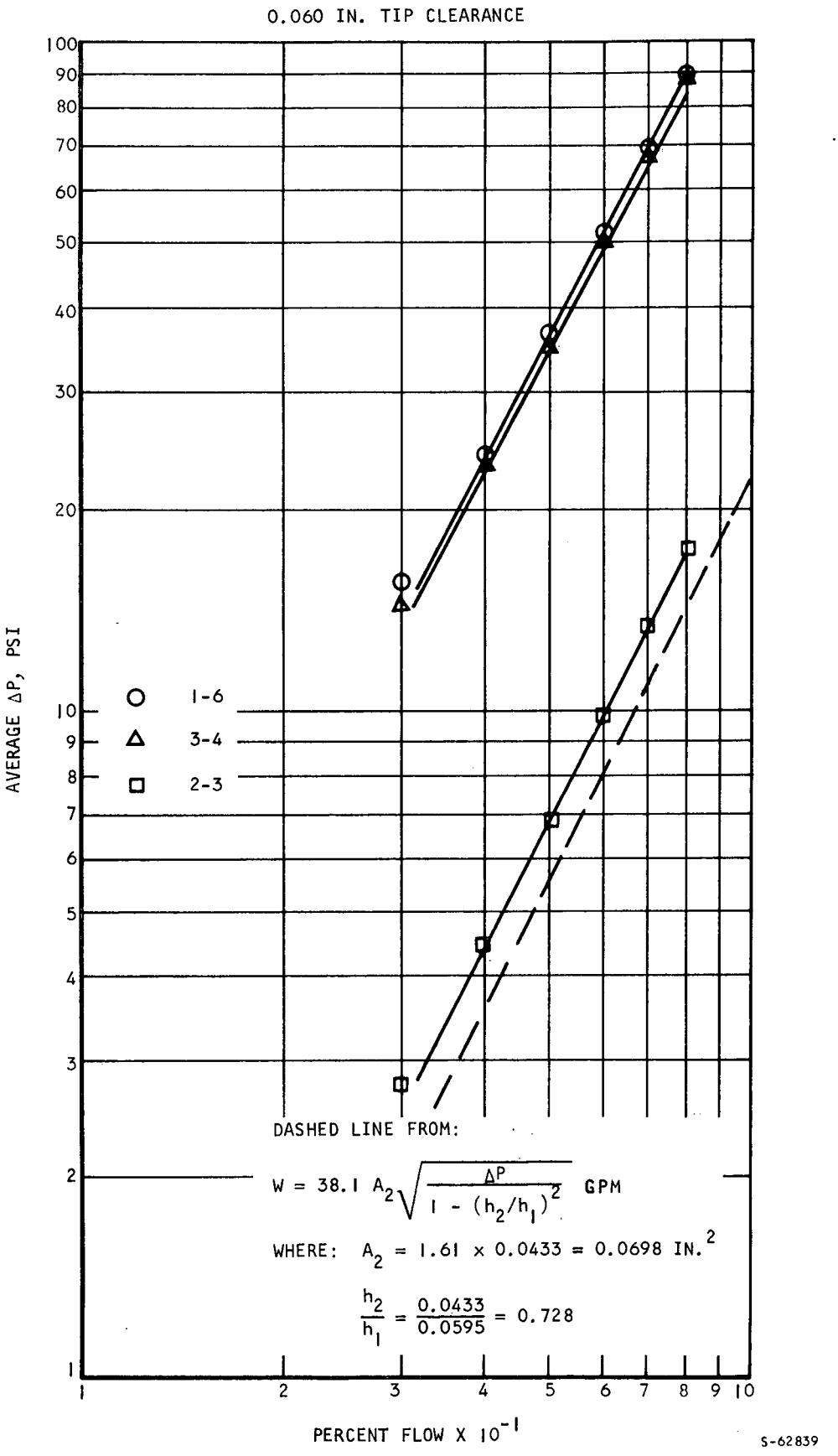

Figure 7-22. Segmented Full-Scale C.L.E. Pressure Drops - No Bypass, Maximum P_6

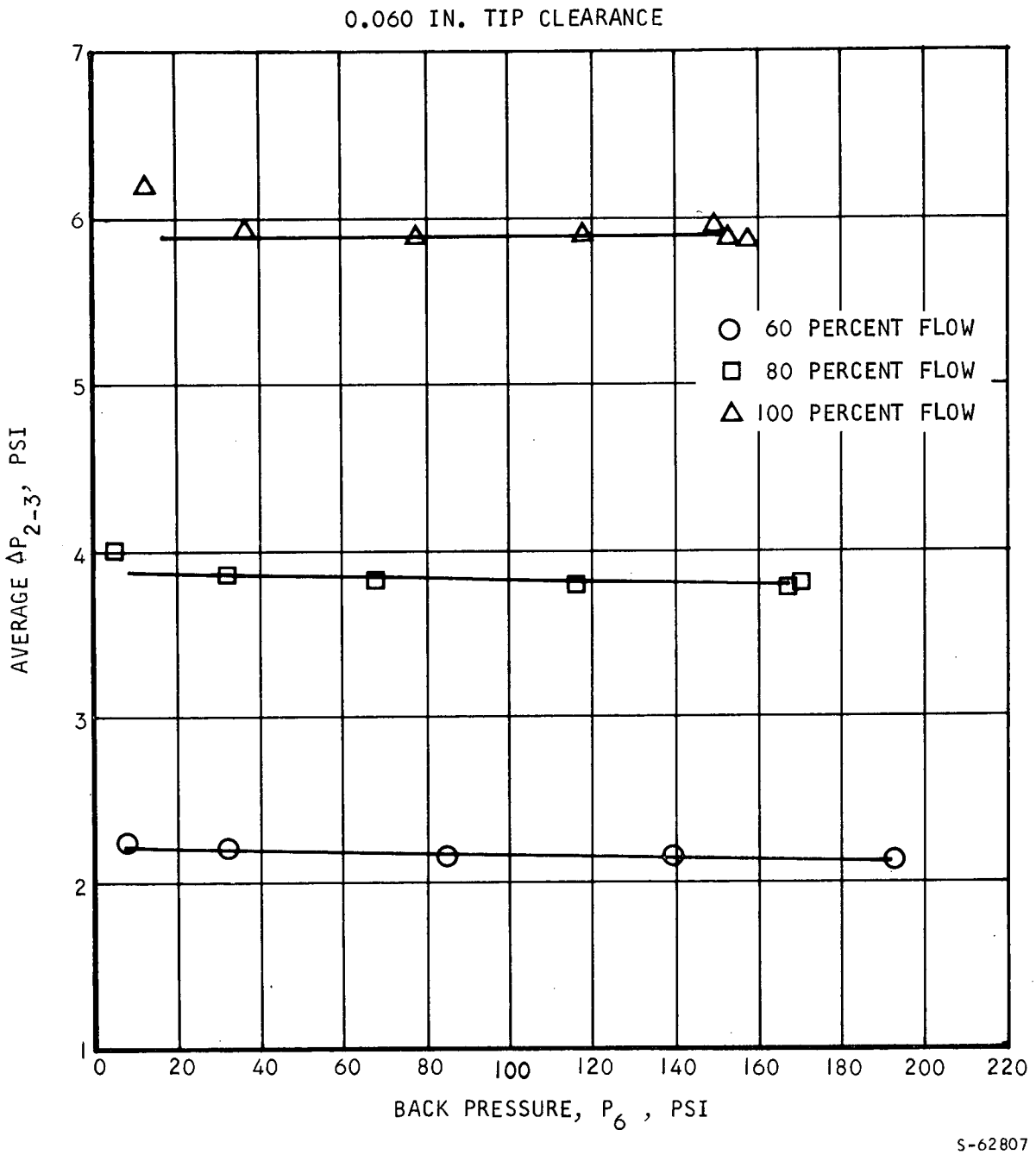

Figure 7-23. Segmented Full-Scale C.L.E. Pressure Drops - With Bypass, Flowmeter ΔP_{2-3} Versus Back Pressure

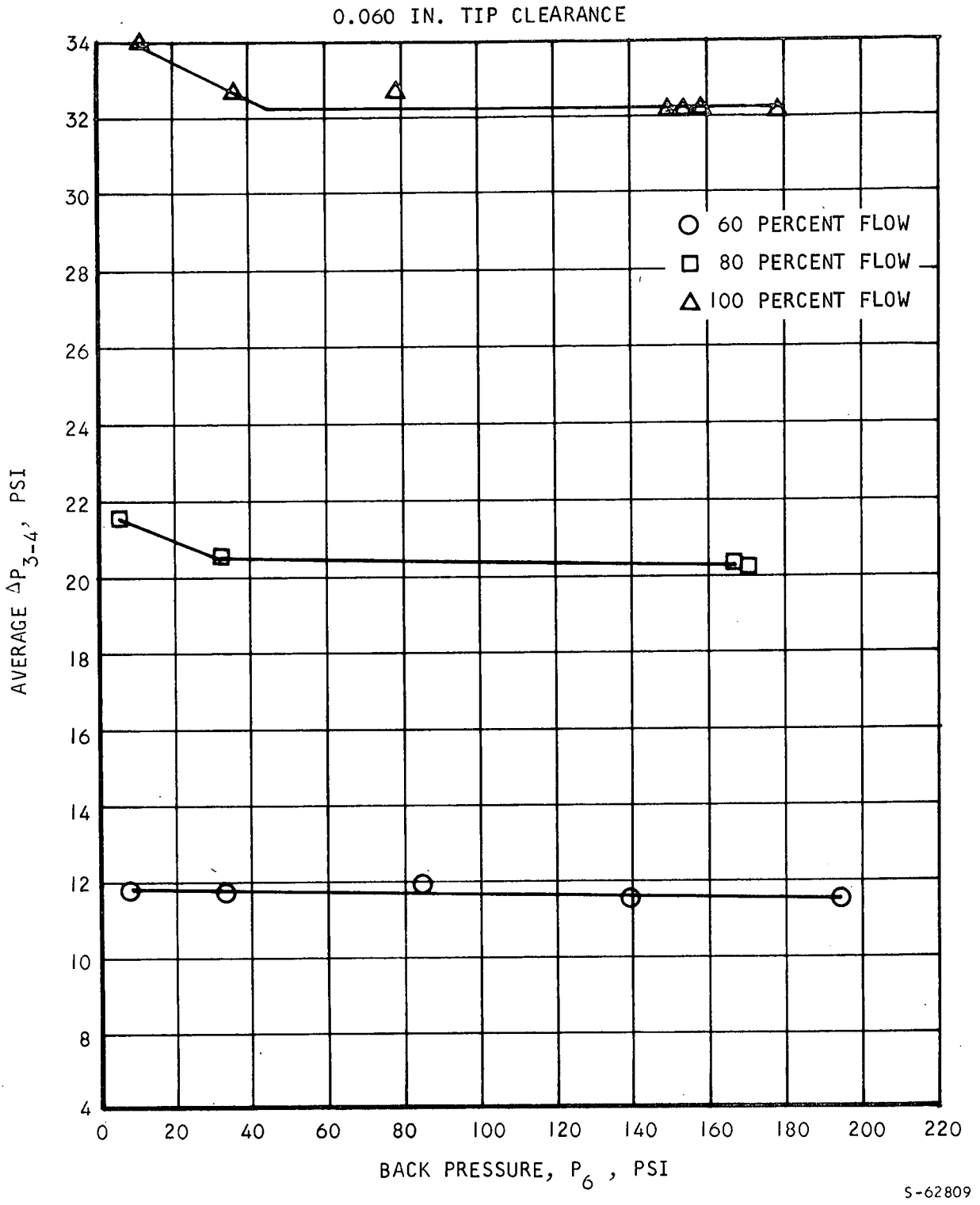

Figure 7-24. Segmented Full-Scale C.L.E. Pressure Drops - With Bypass, Tip ΔP_{3-4} Versus Back Pressure

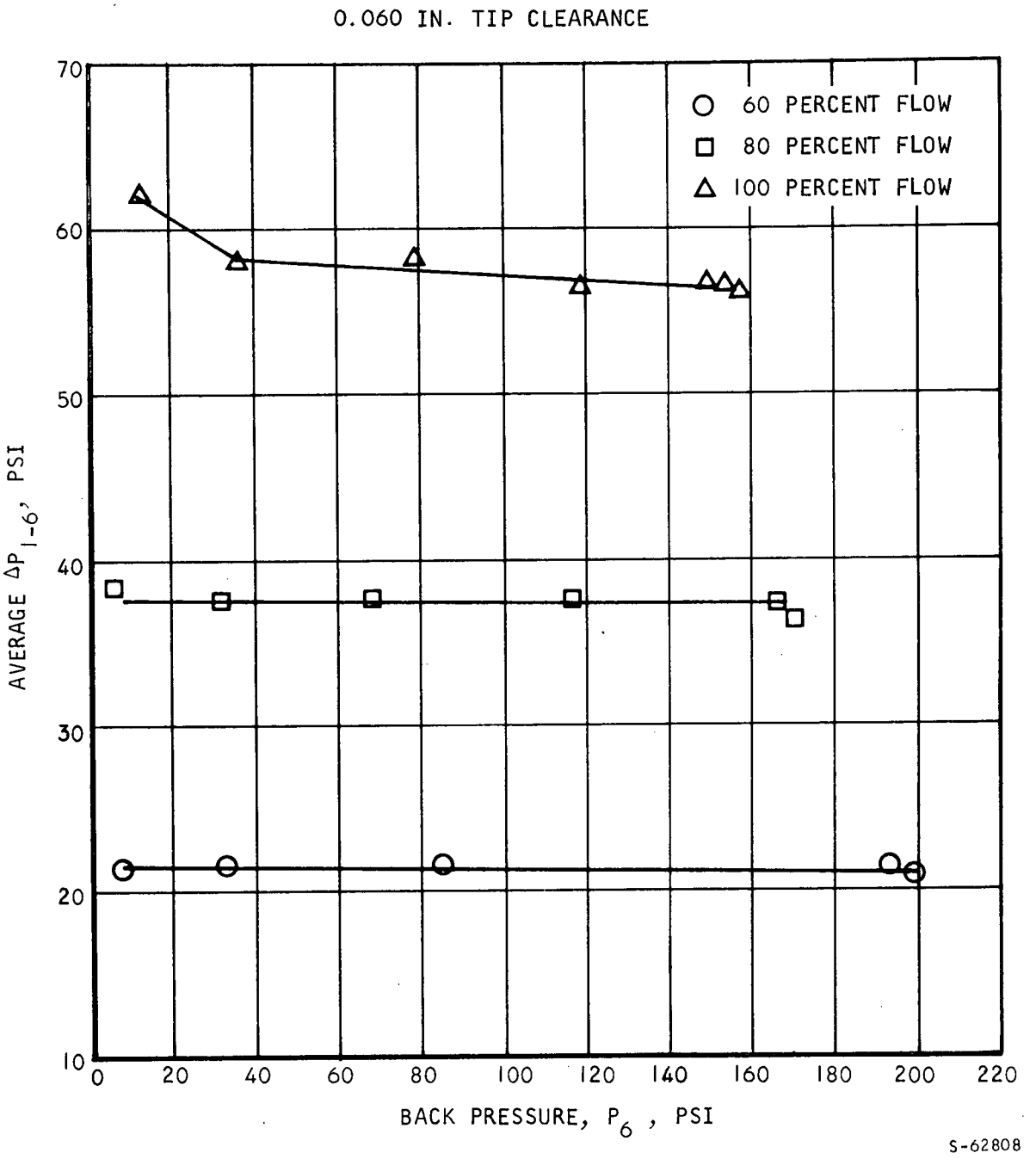

Figure 7-25. Segmented Full-Scale C.L.E. Pressure Drops - With Bypass, Overall ΔP_{1-6} Versus Back Pressure

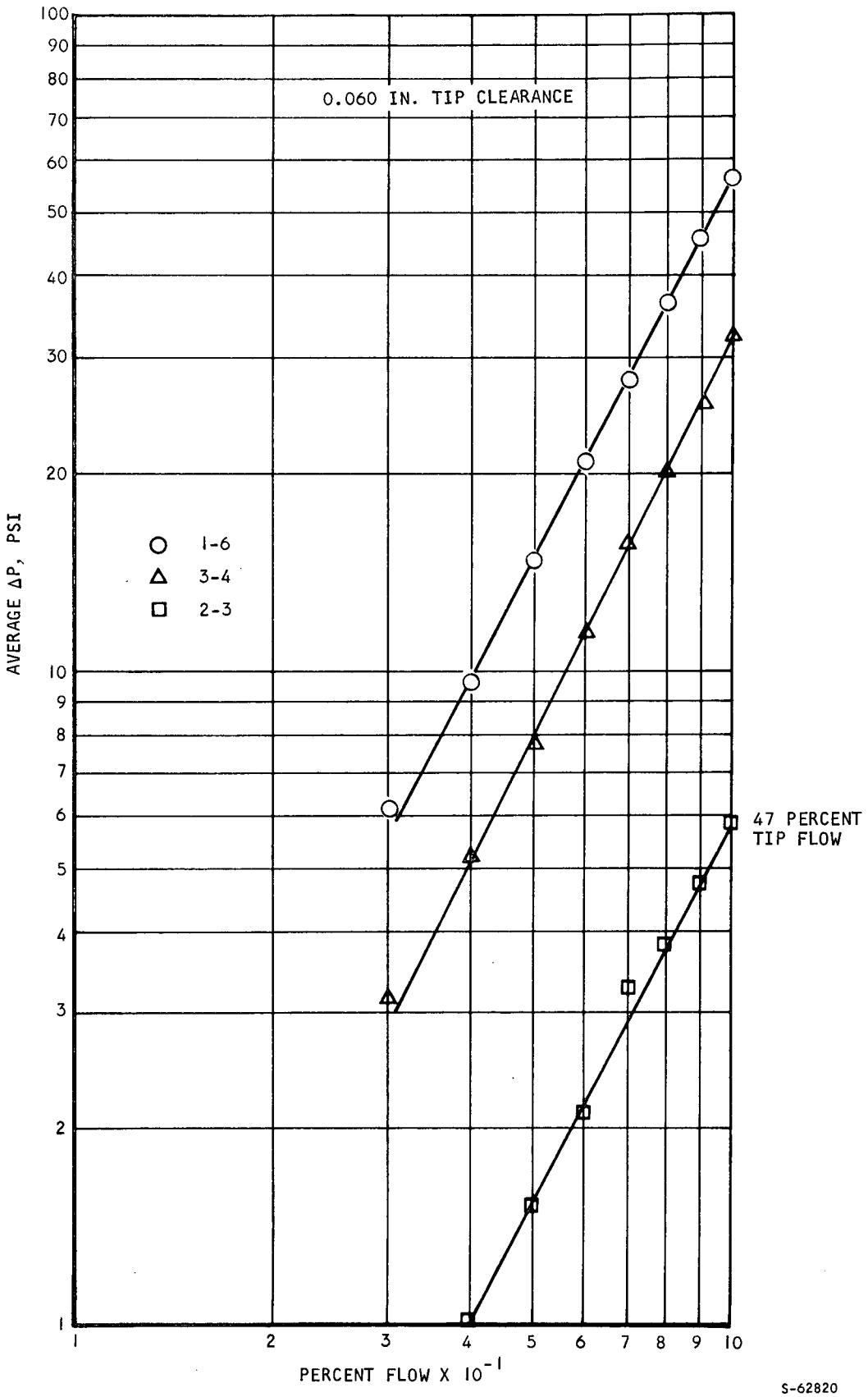

Figure 7-26. Segmented Full-Scale C.L.E. Pressure Drops - With Bypass, Maximum P_6

Instrumentation Location	Flow Divider Location		ΔP, psi (Max. Back Pressure)			
	T, in.	I, in.	100% W	91% W	76% W	60% W
43	0.058	0.034	60	50	34	22
53	0.058	0.036	60	50	34	21
131	0.054	0.041	57	49	34	21
221	0.054	0.038	62	52	37	23
263*	-	-	63	53	37	23
273	0.054	0.039	66	48	32	20
310	0.057	0.040	49	38	22	16
Average	0.056	0.038	60	49	33	21

*Pressure tap at space between two flow-divider segments.

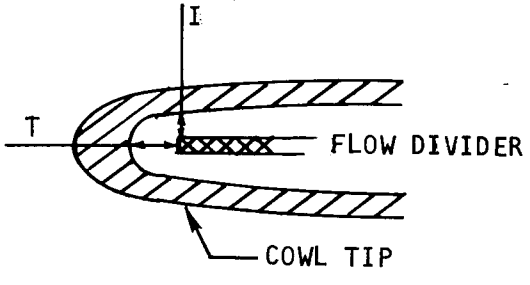

Figure 7-27. Full-Scale Cowl Leading Edge Test Data

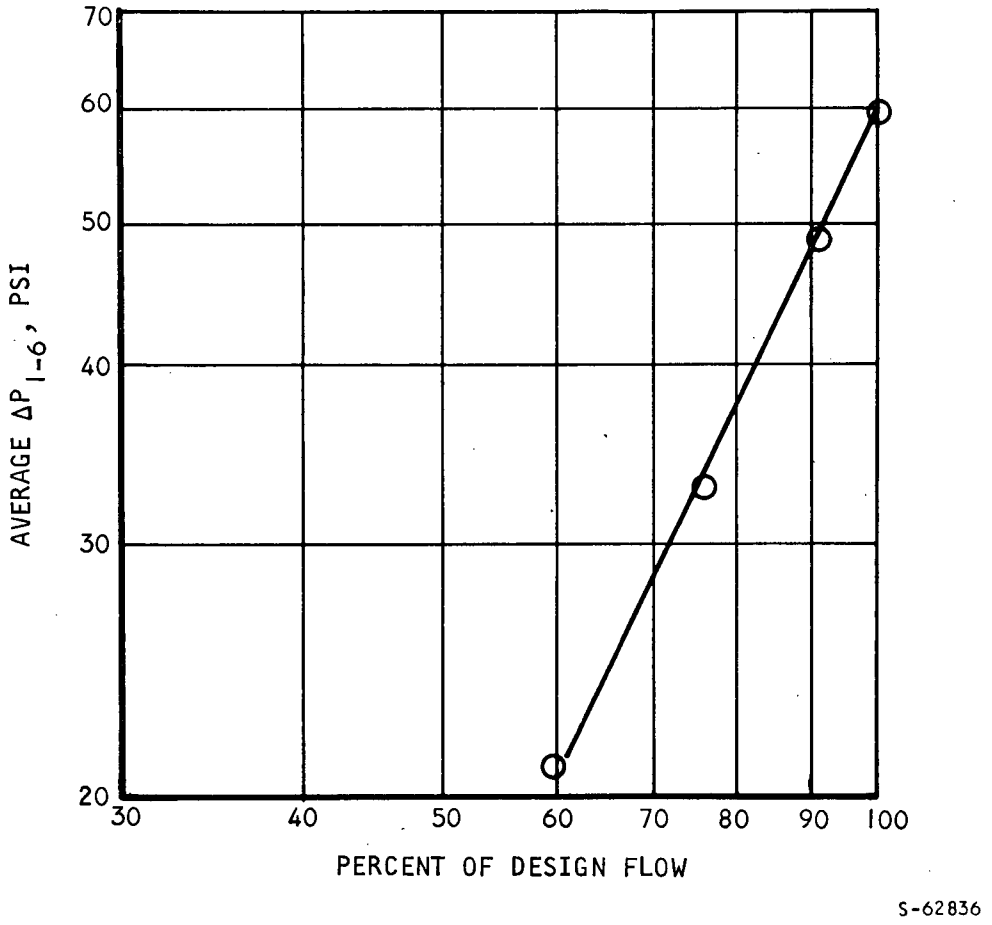

Figure 7-28. Full-Scale Cowl Leading Edge Test Data

TABLE 7-I

SUMMARY OF LEADING EDGE MODEL TEST RESULTS AND PREDICTIONS

Ident No.	Model	Configuration No.	Bypass	A_1, $in.^2$	A_2, $in.^2$	W_3, gpm	W_1, gpm	$\frac{W_1}{W_3} \times 100$, percent	$\frac{W_3}{(W_3)_{Design}} \times 100$, percent	ΔP_{2-3}, psi (in. H_2O)	ΔP_{1-6}, psi (in. H_2O)	Comments
①	10X	1	No	4.4	-	102	102	100	100	(4.4)	(28)	Test results
②	10X	6	Yes	4.4	2.31	102	60.2	59	100	(1.6)	(12.8)	Test results
③	Full-scale segmented	6 (0.041 in. tip)	No	0.066	-	18.3	18.3	100	100	31	148	Test results
④	Full-scale segmented	6 (0.041 in. tip)	No	0.066	-	14.6	14.6	100	80	-	98	Test results
⑤	Full-scale segmented	6 (0.041 in. tip)	No	0.066	-	9.15	9.15	100	50	7.4	41**	Test results
⑥	Full-scale segmented	6 (0.041 in. tip)	No	0.066	-	9.15	9.15	100	50	5.7	36**	Ratioed from ① above
⑦	Full-scale segmented	6 (0.041 in. tip)	Yes	0.066	0.044	18.3	8.1	44**	100	5.6	66**	Test results
⑧	Full-scale segmented	6 (0.041 in. tip)	Yes	0.066	0.044	18.3	9.7	53**	100	-	54**	Ratioed from ② above
⑨	Full-scale segmented	6 (0.050 in. tip)	No	0.0805	-	14.6	14.6	100	80	-	66**	Ratioed from ① above
⑩	Full-scale segmented	6 (0.050 in. tip)	No	0.0805	-	14.6	14.6	100	80	27	76**	Test results
⑪	Full-scale segmented	6 (0.050 in. tip)	Yes	0.0805	0.044	18.3	9.5	52**	100	28	52**	Test results
⑫	Full-scale segmented	6 (0.050 in. tip)	Yes	0.0805	0.044	18.3	10.6	58**	100	-	44**	Ratioed from ② above
⑬	Full-scale segmented	6 (0.050 in. tip)	Yes	0.0805	0.044	18.3	9.0	49**	100	-	55**	Ratioed from ⑦ above
⑭	Full-scale segmented	6 (0.060 in. tip)	No	0.0966	-	18.3	18.3	100	100	27	137	Test results
⑮	Full-scale segmented	6 (0.060 in. tip)	Yes	0.0966	0.044	18.3	8.6	47	100	5.8	56	Test results
⑯	Full-scale full-round	5	Yes	-	-	660	542	82	100	-	77**	Ratioed from ② above
⑰	Full-scale Full-round	5	Yes	-	0.044	660	495*	75*	100	-	81**	Test results
⑱	Full-scale full-round	6 (0.054 in.-0.058 in.)	Yes	-	-	660	-	-	100	-	60**	Test results

* From Figure 7.3 Tenth AIM TDR **Numbers for direct comparison